1  # FOXC2 marks and maintains the primitive spermatogonial stem
2  # cells subpopulation in the adult testis

3  Zhipeng Wang[1,3], Cheng Jin[1,3], Pengyu Li[1], Yiran Li[1], Jielin Tang[1], Zhixin Yu[1], Tao Jiao[1],

4  Jinhuan Ou[1], Han Wang[1], Dingfeng Zou[1], Mengzhen Li[1], Xinyu Mang[1], Jun Liu[1], Yan Lu[1],

5  Kai Li[1], Ning Zhang[2], Shiying Miao[1], Jia Yu[1], Linfang Wang[1] and Wei Song[1]*

6  [1] Department of Biochemistry and Molecular Biology, State Key Laboratory of Medical

7  Molecular Biology, Institute of Basic Medical Sciences Chinese Academy of Medical

8  Sciences, School of Basic Medicine Peking Union Medical College; Beijing, 100005, China.

9  [2] Wellcome Centre for Anti-Infectives Research, Division of Biological Chemistry and Drug

10  Discovery, School of Life Sciences, University of Dundee; Dundee, DD1 5EH, UK.

11  [3] These authors contributed equally: Zhipeng Wang, Cheng Jin.

12  * Correspondence: Wei Song

13

14  **Email:** songwei@ibms.pumc.edu.cn

15  **Author Contributions:** W.S., Z.W. and C.J. conceived and designed the study; Z.W. and C.J.

16  performed most of the experiments and analyzed data with the help of P.L., Y.L., and J.T.;

17  Z.Y., T.J., J.O., H.W., D.Z., M.L., X.M., J.L., Y.L., and K.L. provided additional experimental

18  support; J.Y., N.Z., S.M. and L.W. provided critical suggestions on manuscript preparation;

19  W.S., Z.W., and C.J. wrote the manuscript with help from all authors.

20  **Competing Interest Statement:** The authors declare that they have no competing interests.

21  **Classification:** BIOLOGICAL SCIENCES and Developmental Biology

22  **Keywords:** FOXC2; Spermatogonial stem cells; quiescent

23  **This PDF file includes:**

24  Main Text
25  Figures 1 to 7
26  Supplemental Figures S1 to S6
27  Captions for Supplemental Tables S1 to S4
28  Supplemental Materials and Methods
29
30

## Abstract

In adult mammals, spermatogenesis embodies the complex transition from spermatogonial stem cells (SSCs) to spermatozoa. This process is initiated by the dynamic transition among a series of SSCs subpopulations. However, it remains elusive and controversial for the identity of the primitive adult SSCs at the top of this developmental hierarchy. Using single-cell analysis and lineage tracing, we identified forkhead box protein C2 (FOXC2) as a specific marker for the primitive SSCs subpopulation in adult mice and humans. During homeostasis, FOXC2$^+$-SSCs can initiate spermatogenesis, and through which give rise to all sets of spermatogenic progenies. Specific ablation of the FOXC2$^+$-SSC results in depletion of the undifferentiated spermatogonia pool. During germline regeneration, spermatogenesis can be completely restored by FOXC2$^+$-SSCs. Germ cell-specific *Foxc2* knockout resulted in accelerated exhaustion of SSCs and eventually led to male infertility. Mechanistically, FOXC2 is required for maintaining the quiescent state of the primitive SSCs by promoting the expression of negative regulators of cell cycle phase transition. Overall, this work proposed FOXC2$^+$-SSCs as an indispensable and primitive subgroup during homeostasis and regeneration in the adult testis.

## Introduction

Through spermatogenesis, spermatozoa are generated from spermatogenic cells that are originated from spermatogonial stem cells (SSCs). It is critical for this process to be continuous and successful that SSCs are maintained in a homeostatic balance between self-renewal and differentiation (1). The SSCs, as the least differentiated spermatogonia, belong to a subgroup of undifferentiated spermatogonia (uSPG) that are morphologically categorized into three subtypes, i.e., A$_{single}$ (A$_s$), A$_{paired}$ (A$_{pr}$), and A$_{aligned}$ (A$_{al}$) cells (2). So far, three models have been proposed for the mechanism underlying SSCs' self-renew based on the dynamic transitions among subgroups. In the 'A$_s$ model', A$_s$ spermatogonia serve as SSCs that are capable of both self-renew and further transformation into A$_{pr}$ and A$_{al}$ that eventually give rise to spermatogonia (3, 4). Later, based on the discovery of Ngn3 and Gfrα1 as SSCs markers, the 'fragmentation model' suggests all three subgroups with stem cell potential and the SSCs renewal is achieved through the fragmentation of pairs and chains (5). Further work on SSCs markers such as ID4 and PAX7 inspired the 'hierarchical A$_s$ model', in which only specific A$_s$ spermatogonia possess the potential for long-term self-renewal whereas the majority are restricted in their capacity (6, 7). Though their standing points of view differ, each model seems well supported by the respective collection of evidence, which to some extent reflects the nature of heterogeneity and dynamics among SSCs subpopulations.

In recent years, great insights into SSCs behaviors and regulations have been provided by a body of pioneer works, especially with recent advances in single-cell gene-expression profiling, highlighting great heterogeneity of SSCs and focusing on characterizing the nature of SSCs states especially for seeking the primitive subgroup among them. Within the population of uSPG, a number of genes relatively higher expressed in primitive subfractions have been identified and well investigated, i.e., Gfra1, ID4, Ret, Eomes, Pax7, Nanos2, Shisa6, T, Pdx1, Lhx1, Egr2 and Plvap (5-15). Particularly, Gfra1, ID4, Eomes, Pax7, Nanos2, and Plvap are further validated as the SSCs markers through lineage tracing experiment, which is considered to be a reliable method to study the origin and development of stem cells. However, some essential and primitive sub-populations

74    remain undiscovered, and the identification of which is of great significance for elucidating the

75    developmental process of SSCs renewal and its behavior in testis.

76       Adult stem cells (ASCs), as the undifferentiated primitive cells that can be found in nearly all

77    types of tissues in mammals, are characteristic for a unique quiescent status reflected by both

78    reversible cell cycle arrest and specific metabolic alterations (16). Putative the primitive SSCs

79    subgroups appear to share this characteristic, as revealed in recent single-cell RNA-sequencing

80    (scRNA-seq) analysis in humans and mice, being largely non-proliferative while capable of

81    reciprocating between the quiescent and activated status (17-21). However, rigorous biological

82    validation of these populations is lacking through live imaging or genetic lineage tracing, or other

83    means. On the other hand, cells in a quiescent state are supposed to be more resilient to genotoxic

84    insults, which shall enable the primitive SSCs to sufficiently restore spermatogenesis upon such

85    disturbance.

86       Here, we identified a subpopulation of adult SSCs specifically marked by forkhead box protein

87    C2 (FOXC2). In adult mice, spermatogenic cells derived from the FOXC2$^+$ population were able to

88    complete the whole spermatogenesis. Upon the loss of this specific subpopulation of SSCs, the

89    undifferentiated spermatogonia pool was exhausted, eventually leading to defective

90    spermatogenesis. Specifically, FOXC2 is required for maintaining SSCs quiescence by promoting

91    the expression of negative regulators of cell cycle phase transition, thus symbolizing the primitive

92    state of these adult SSCs. Moreover, the FOXC2$^+$ population endured the chemical insult with

93    busulfan and effectively restored spermatogenesis, thereby critical for keeping the reproductive

94    homeostasis in male adult mice. Thus, our results demonstrate that FOXC2 marks the primitive

95    SSCs subpopulation in the adult testis, and is also required for the homeostasis and regeneration

96    of SSCs.

## Results

**Identification of FOXC2$^+$-SSCs as the quiescent and developmental starting point of adult uSPG.** We performed single-cell RNA-seq (10x genomics) of the uSPG from adult mice testes marked by THY1, a widely recognized surface marker for uSPG with self-renewing and transplantable state (22, 23), to dissect the heterogeneity and developmental trajectory (Fig.1A, Fig. S1A, B). Among 5 distinct clusters identified, Cluster1 was characterized by the high expression of stemness markers whereas other clusters were featured by progenitor or differentiating spermatogonia (dSPG) markers (Fig.1B, Fig. S1C, D). Primarily mapped to the extreme early point of the developmental trajectory, Cluster1 cells appeared quiescent and likely represented the primitive state of uSPG populations (Fig.1B, Fig. S1E-G). The top10 differentially expressed genes (DEGs) associated with Cluster1 are featured by SSCs markers such as *Mcam* (24), *Gfra1* (5), *Tcl1* and *Egr2* (12, 18) (Fig.1C, Fig. S2A, Supplemental Table S1) in addition to six others expressed in different stages of germ cells and/or somatic cells, in which only FOXC2 was exclusively localized in the nucleus of a subgroup of ZBTB16$^+$ uSPG (25, 26) in mice (Fig. 1D, Fig. S2B). More specifically, in adult mice, FOXC2 displayed differential expressions among various subtypes of uSPG, being more specific in A$_s$ (59.9%) than other subtypes including A$_{pr}$ (5.2%), A$_{pr-1}$ (4.1%), A$_{al4-1}$ (1.83%), A$_{al8-1}$ (1.5%), and A$_{al16-1}$ (1.67%) (Fig. 1E). There was only a small fraction (5.1%) was active in proliferation as indicated by MKI67 (Fig. 1F), suggesting that FOXC2$^+$ cells are primarily quiescent. Additionally, when examining the SSCs markers validated previously by lineage tracing (27), we found that FOXC2 displays a higher level of co-localization with GFRA1 and EOMES than PAX7 and NEUROG3 (28), indicating the FOXC2$^+$ cells contain but differ from the known SSCs subsets (Fig. 1G).

We next analyzed the expression of FOXC2 in adult human testis using the published scRNA-seq dataset (17) (GSE112013). As expected, FOXC2 was also specifically expressed in the human SSCs, most of which were MKI67$^-$ (Fig. 1H, Fig.S2C). Pseudotime analysis showed that the FOXC2$^+$ cells located at the start of the developmental trajectory with a proportion of about 90% that were MKI67$^-$ (Fig. 1I). Immunofluorescence staining confirmed that FOXC2$^+$ cells were a subset of ZBTB16$^+$ spermatogonia in adult human testis, and most of them were MKI67$^-$ (Fig. 1J), possibly representing the A$_{dark}$ SSCs also known as the reserve stem cells or 'true SSC' in human testis(29-33). These results suggested that FOXC2 was similarly expressed in the SSCs of adult human and mouse testis and may possess a conserved function.

**FOXC2$^+$-SSCs can sufficiently initiate and sustain spermatogenesis.** We generated *Foxc2*$^{CRE/+}$;*R26T/G*$^{f/f}$ mice in which FOXC2$^+$ cells were specifically labeled with GFP to enable the progeny tracing after tamoxifen treatment (Fig. S3A) (34). Tamoxifen was introduced at 2-month of age, after which the FOXC2-expressing lineage (GFP$^+$) was tracked at d3 (day3), w1 (week1), w2, w4, w6, m4 (month4), m7, and m12 respectively (Fig. 2A). At d3, the tracked cells were both GFP$^+$ and FOXC2$^+$ (Fig. 2B) and constituted 0.027% of the total testicular cells as indicated by the fluorescence-activated cell sorting (FACS) analysis (Fig. 2C). FACS-sorted GFP$^+$ cells were then transplanted into testes of recipient mice pre-treated with busulfan, in parallel to THY1$^+$ cells derived from *eGFP*$^{Tg/+}$ mice as control. Two months after transplantation, FOXC2$^+$ cells generated 5 times greater number of colonies than the THY1$^+$ control (Fig. 6D, E), indicating that the FOXC2$^+$ cells possess higher stemness as convinced by stronger transplantable viability.

At w1, all GFP$^+$ cells were identified as uSPGs, encompassing A$_s$, A$_{pr}$, and A$_{al-4}$ (Fig. 2F$_a$). Specifically, FOXC2$^+$ A$_s$ gave rise to 3 types of A$_{pr}$, i.e., FOXC2$^+$/FOXC2$^+$, FOXC2$^+$/FOXC2$^-$, and FOXC2$^-$/FOXC2$^-$ (Fig. 2F$_{c1, b, c2, d2}$), which then either produced FOXC2$^+$ or FOXC2$^-$ A$_s$ through

4

144     symmetric or asymmetric division (Fig. 2F$_{c3, d1, f1}$), or developed into A$_{al}$ with no more than one
145     FOXC2$^+$ cell in the chains (Fig. 2F$_{e, f2}$). These results confirmed that FOXC2$^+$ cells were capable
146     of self-renewal to sustain the population as well as replenishing the uSPG pool by producing
147     downstream progenies, thereby serving as primitive SSCs. In the following 2-6 weeks, GFP$^+$
148     colonies further expanded and produced GFP$^+$ sperms in the epididymis, from which healthy GFP$^+$
149     offspring were given birth by C57 female recipients (Fig. 2G). The GFP$^+$ colonies constituted
150     83.67%, 90.48%, 96.78%, 98.55%, and 99.31% of the total length of the seminiferous tubules at
151     w6, m2, m4, m7, and m12 respectively (Fig. 2H, I). All offspring were GFP$^+$ from m4 onwards (Fig.
152     2J). Additionally, the EOMES$^+$, GFRA1$^+$ and PAX7$^+$ cells were all GFP$^+$ at w2, further confirming
153     these progenies were derived from the FOXC2$^+$ cells (Fig. 2K). Overall, FOXC2$^+$-SSCs can produce
154     all subtypes of uSPG, thus initiating spermatogenesis in adult mice.
155
156     **Specific ablation of the FOXC2$^+$-SSC results in depletion of the uSPG pool.** We then prepared
157     *Foxc2$^{Cre/+}$;R26$^{DTA/+}$* mice to investigate the physiological requirement of FOXC2$^+$-SSCs in
158     spermatogenesis (34). FOXC2$^+$ population in 2-month-old mice was specifically ablated with
159     tamoxifen-induced diphtheria toxin (DTA). The testes of these mice were examined at day3, day7,
160     and day14 post tamoxifen induction (Fig. 3A). Gradual loss of weight in testes coincided with the
161     reduction in the size of testes in all the mice while body weight was maintained (Fig. 3B, C).
162     Specifically, at d3, there were no detectable FOXC2$^+$ cells in addition to the decrease in the number
163     of GFRA1$^+$, LIN28A$^+$ (35) and ZBTB16$^+$ uSPG at the basement membrane of seminiferous tubules;
164     at d14, all GFRA1$^+$, LIN28A$^+$ and ZBTB16$^+$ uSPG disappeared while vacuoles formed at the
165     basement membrane with remaining spermatocytes and spermatids in the seminiferous lumen
166     (Fig. 3D–F, Fig. S3B). Meanwhile, the expression of DDX4 (36) and DAZL (37) as germ cell
167     markers was significantly reduced along with nearly undetectable expression of uSPG markers
168     such as ZBTB16, LIN28A, GFRA1, RET, and NEUROG3 (28) (Fig. 3G). These results indicate an
169     uSPG exhaustion as the result of the FOXC2$^+$-SSCs ablation, therefore supporting the critical role
170     in spermatogenesis played by FOXC2$^+$ population.
171
172     **FOXC2$^+$-SSCs are resilient to genotoxin and indispensable for germline regeneration.** Next,
173     we examined the regenerative viability of FOXC2$^+$-SSCs. At d20 post busulfan treatment
174     (20mg/kg), FOXC2$^+$ cells constituted the majority of uSPGs (Fig. 4A). Following a sharp decrease
175     in cell number in the first five days, ZBTB16$^+$ and GFRA1$^+$ cells began to recover from d25 while
176     the number of FOXC2$^+$ cells remained stable (Fig. 4B), indicating that this population is insensitive
177     to busulfan. We then checked changes in the proportion of MKI67$^+$ cells, active in proliferation, in
178     FOXC2$^+$ population after busulfan treatment (Fig. 4C, D). At d30, the MKI67$^+$ proportion rose to
179     15.92%, indicating a higher level of proliferation, albeit the total cell number stayed static (Fig. 4B,
180     D), thereby becoming the driving force in restoring spermatogenesis. Up to d120, the MKI67$^+$
181     proportion had settled gradually back to the pre-treatment level, accompanied by the full recovery
182     of spermatogenesis (Fig. 4D). Further details of this process were revealed during lineage tracing
183     (Fig. 4E). Three days after tamoxifen induction, the 2-month-old *Foxc2$^{CRE/+}$;R26T/G$^{f/f}$* mice were
184     treated with busulfan. Consistent with the results above, at d20, the survived uSPG were
185     predominantly GFP$^+$ (Fig. 4F). Over 68.5% of the total length of the seminiferous tubules were GFP$^+$
186     at m2, and this proportion rose to 95.43%, 98.41%, and 99.27% at m4, m7, and m12 respectively
187     (Fig. 4G, H), which was comparable to the proportion by tamoxifen induction alone (Fig. 2I). From
188     m4 onwards, nearly all germ cells, spermatids, and their offspring were GFP$^+$ (Fig. 4G, I). Together,

189  these results confirmed that FOXC2$^+$-SSCs are indispensable for germline regeneration that is
190  central to spermatogenesis recovery from interruptions.
191
192  **FOXC2 is essential for SSCs maintenance in adult mice.** We then focused on dissecting
193  FOXC2's role in the SSCs maintenance using *Foxc2$^{f/-}$;Ddx4*-cre mice (38) (Fig. 5A). No significant
194  difference was observed in the expressions of various uSPG markers, including ZBTB16 and
195  LIN28A, between *Foxc2$^{f/-}$; Ddx4*-cre and *Foxc2$^{f/+}$* mice at the age of 1 week (Fig. S4B). However,
196  adult *Foxc2$^{f/-}$;Ddx4*-cre mice displayed clear testis weight loss without significant body weight loss
197  (Fig. 5B, C). Moreover, in these mice, we observed severe degeneration of seminiferous tubules,
198  reduced number of spermatids in the epididymis, and decreased size of the uSPG population with
199  age (Fig. 5D–G) but without apparent signs of apoptosis (Fig. S5B). The 6-month-old *Foxc2$^{f/-}$;Ddx4*-
200  cre mice were infertile, in which over 95% seminiferous tubules were Sertoli-only with hardly
201  detectable expressions of DAZL, DDX4, LIN28A, and ZBTB16 (Fig. 5D–F, H). Therefore, FOXC2
202  is essential for maintaining the SSCs homeostasis and normal spermatogenesis in adult mice.
203
204  **FOXC2 maintains the SSCs homeostasis via negative regulation of cell cycle.** We collected
205  THY1$^+$ uSPGs from 4-month-old *Foxc2$^{f/+}$* and *Foxc2$^{f/-}$; Ddx4*-cre mice and compared their
206  transcriptome signatures revealed from scRNA-seq (Fig. 6A). The pseudotime analysis identified
207  Cluster1, which represented the FOXC2-expressing SSCs in *Foxc2$^{f/+}$* mice corresponding to the
208  FOXC2-deleting SSCs in the *Foxc2$^{f/-}$; Ddx4*-cre mice, was specifically assigned to the extremely
209  early stage of the development trajectory in respective samples, which was validated by the
210  expression of corresponding markers (Fig. 6B, Fig. S5A, B). Aggregated analysis of the overall
211  uSPG populations showed that cells derived from *Foxc2$^{f/-}$; Ddx4*-cre mice were specifically
212  associated with the late stage of the development trajectory, as opposed to *Foxc2$^{f/+}$* mice where
213  nearly all the cells derived were concentrated at the early stage of development (Fig. 6C, Fig. S5C).
214  This implies that the loss of Foxc2 prompts the SSCs to progress into a more differentiated stage
215  with defection in maintaining the primitive identity of SSCs. Further analysis of the cells in Cluster1
216  revealed two distinct subclusters, i.e., Subclusters0 and Subclusters1 (Fig. S6A). Formed primarily
217  by the Cluster1 cells derived from *Foxc2$^{f/+}$* mice, Subclusters0 was featured by stemness markers,
218  while Subcluster1, representing the majority of Cluster1 cells from *Foxc2$^{f/-}$; Ddx4*-cre mice, was
219  featured by progenitor markers (Fig. S6B, C). Consistently, pseudotime analysis showed that
220  Cluster1 cells from *Foxc2$^{f/+}$* mice projected a forward stage of the developmental trajectory
221  indicated by stemness markers, whereas Cluster1 cells from *Foxc2$^{f/-}$; Ddx4*-cre mice were
222  associated with a later stage of the developmental trajectory (Fig.6D, Fig. S6D, E). More
223  specifically, less number of cells were found at the starting state1 in Cluster1 from *Foxc2$^{f/-}$; Ddx4*-
224  cre mice than in *Foxc2$^{f/+}$* mice, with rather more cells in the developmental progression (from state1
225  to state5), especially at the advanced state5 (Fig. 6E). Thus, FOXC2 deletion caused defective
226  SSCs maintenance and committed the primitive SSCs to a differentiation destiny. Further, there
227  were 932 genes down-regulated in Cluster1 cells derived from *Foxc2$^{f/-}$; Ddx4*-cre mice in
228  comparison to *Foxc2$^{f/+}$* mice (Fig. 6F, Supplemental Table S2), which were functionally associated
229  with both stem cell population maintenance and mitotic cell cycle (Fig. 6G). Consistently, the GSEA
230  analysis revealed a more progressive cell cycle in Cluster1 upon *Foxc2*-knockout (Fig. 6H),
231  confirming the role of FOXC2 in regulating the cell cycle of the primitive SSCs.
232  We then performed Cleavage Under Targets and Tagmentation (CUT&Tag) sequencing to
233  explore the underlying mechanism (39, 40), for which GFP$^+$ SSCs from *Foxc2$^{CRE/+}$;R26T/G$^{f/f}$* mice
234  3 days after tamoxifen induction, representing the FOXC2$^+$-SSCs, were isolated for CUT&Tag
235  sequencing (Fig. 7A). Specific peaks enriched in the promoter region of 3629 genes (Fig. 7B, C;

236 Supplemental Table S2) showed functional enrichment in biological processes such as DNA repair
237 and mitotic cell cycle regulation (Fig. 7D). By overlapping with the 932 genes down-regulated in
238 Cluster1 cells from *Foxc2*$^{f/-}$; *Ddx4*-cre mice, we obtained 306 genes as the candidates subjective
239 to the regulation by FOXC2 (Fig. 7E; Supplemental Table S2). Further, GO enrichment analysis of
240 these genes highlighted a distinctive functional cluster (11 genes) focusing on the negative
241 regulation of cell cycle (Fig. 7F; Supplemental Table S3) (41-50). More specifically, significant
242 peaks enrichment at the promoter region were observed for these candidate genes (Fig. 7G).
243 Meanwhile, as predicted using the JASPAR Scan function (binding potential >0.8), there showed
244 strong binding potential of FOXC2 towards these candidate genes (Fig. 7I) via the binding motif of
245 FOXC2 (Fig. 7H), which was further confirmed by the results from the CUT&Tag qPCR (Fig. 7J).
246 Overall results implied that FOXC2 may function as a gatekeeper that ensures the quiescent state
247 of the primitive SSCs by impeding cell cycle progression.
248
249 **Discussion**
250
251 In this work, a comprehensive analysis of uSPG populations with scRNA-seq and the following
252 lineage tracing study by whole-mount immunofluorescence assay led to the identification of
253 FOXC2-expressing SSCs as an important and primitive SSCs subpopulation in adult mice. Further
254 investigation through functionality analysis confirmed FOXC2 is essential for SSCs self-renewal
255 and stemness, thereby is required for maintaining the SSCs population that is critical for continuous
256 spermatogenesis. Importantly, our data demonstrated that the colonies formed by FOXC2$^+$ cells
257 constituted nearly the total length of the seminiferous tubules (99.31%), implying that the FOXC2$^+$-
258 SSCs can support the complete spermatogenesis in adult mice.
259 GFRA1$^+$ A$_{pr}$ and A$_{al}$ cells were found to break randomly and a portion of them can return to the
260 stem cell state (5). Interestingly, our findings showed FOXC2 appeared in one of the A$_{pr}$ or A$_{al}$ cells
261 at times, therefore raising a possibility that the subset of GFRA1$^+$ cells that return to stem cell state
262 after intercellular bridge break, maybe FOXC2$^+$ due to different cell cycle state. If so, based on both
263 findings, GFRA1$^+$FOXC2$^+$ could represent a quiescent state whereas GFRA1$^+$FOXC2$^-$ is proliferate
264 active, which certainly requires further validation possibly through multiple lineage tracing and live
265 imaging.
266 We observed that the FOXC2$^+$-SSCs were almost all in a non-proliferative state (~94.9%), and
267 further revealed that FOXC2 functioned in the negative regulation of cell cycle progression, thus
268 confirming that FOXC2-expressing SSCs are quiescent SSCs population in adult mice. The finding
269 that FOXC2 inhibited cell cycle and differentiation of SSCs in testis is consistent with that reported
270 in other tissues (51, 52). In general, the quiescent state is a protective mechanism for stem cell
271 storage and prevents stem cells from damage or depletion under genotoxic stresses (1, 53-55). In
272 our work, after the busulfan treatment, the quantity of FOXC2$^+$ cells remained stable and the
273 survived uSPGs were predominantly FOXC2$^+$, indicating its insensitivity to cytotoxic agents.
274 However, the proportion of MKI67$^+$FOXC2$^+$ cells increased by 15.92% after 30 days of the busulfan
275 treatment and decreased back to the pre-treatment level (5.08%) at 120 days, implying that the
276 quiescent FOXC2$^+$ cells were able to transform into the proliferative FOXC2$^+$ cells to replenish the
277 SSCs pool to maintain the SSCs homeostasis and normal spermatogenesis. We further confirmed
278 by lineage tracing analysis that FOXC2-expressing cells were the only remaining SSCs population
279 and were responsible for germline regeneration after the busulfan treatment, indicating that
280 FOXC2$^+$-SSCs represent a functionally important stem cell population with regenerative ability. In
281 the future, more insights into the unique regulation of SSCs can be drawn from studying and

282 comparing the transition between the quiescent and proliferative states in FOXC2$^+$ and other SSCs
283 subpopulations.

284 According to our findings, we proposed a model for the maintenance of the FOXC2+ SSCs
285 subpopulation (Fig. 7K). Under physiological conditions, FOXC2$^+$ A$_s$ cells (including
286 FOXC2$^+$GFRA1$^+$, FOXC2$^+$EOMES$^+$ cells, etc.) constitute the primitive population of SSCs, of which
287 only a small proportion (~5.1%) cells are proliferative while the majority remains quiescent (Fig.
288 7Ka). This primitive population can divide symmetrically or asymmetrically into different A$_{pr}$ and A$_{al}$
289 (Fig. 7Kb). Then FOXC2$^+$ cells (Fig. 7Kb) may break from the syncytial and return to A$_s$ state (Fig.
290 7Ka) to maintain the stable number of the primitive SSCs. FOXC2$^-$ progenies, derived from the
291 FOXC2$^+$ primitive population, form a transit amplification (TA) SSCs pool (Fig. 7Kc) to support
292 spermatogenesis. However, it requires continuous supply from the FOXC2$^+$ population and is
293 subject to exhaustion when the supply is disrupted. In the context of regeneration conditions, the
294 FOXC2$^+$MKI67$^-$ cells can survive and set out the recovery process (Fig. 7Kd). At the early stage,
295 increasing proportions of FOXC2$^+$MKI67$^-$ cells are committed to transforming into proliferative
296 FOXC2$^+$MKI67$^+$ cells, strengthening the supply to the TA SSCs pool (Fig. 7Ke). At the late recovery
297 stage, MKI67$^+$/MKI67$^-$ ratio returns to the physiological level in FOXC2$^+$ population (Fig. 7Ka),
298 leaving the total number of FOXC2$^+$ cells stable therefore maintaining the SSCs homeostasis.
299 However, it is necessary to perform more investigation to further improve and modify this model to
300 gain a complete understanding of the connections between different primitive SSCs subpopulations
301 via lineage tracing assays in the testes of adult mice.

302 Based on our observation, FOXC2 seems nonessential for the transformation from gonocytes to
303 SSCs in infant mice, in contrast to its requirement for adult spermatogenesis. A recent study
304 showed that FOXC2 was present in a fraction of A$_8$ and A$_{16}$ cells in the postnatal mouse testis (<5
305 weeks), however, this FOXC2$^+$ subpopulation appeared more active in proliferation than the adult
306 counterpart (56). Such differential functionality might reflect the difference in the physical nature of
307 spermatogenesis between developmental stages. For example, the maturity of spermatogenesis
308 is still under development during the juvenile period with a focus on expanding the SSCs pool.
309 Therefore, it would be interesting to explore differences in individual functional contexts as well as
310 the underlying regulatory mechanisms. Meanwhile, FOXC2, highly conserved between mice and
311 humans with 94% identity in amino acid sequence (57), is also expressed in a subset of human
312 adult SSCs, raising the possibility of an evolutionarily conserved mechanism governing SSCs
313 homeostasis in humans. Further work following this direction might be of great clinical significance
314 specifically to patients who suffer from infertility. Moreover, the developmental correlation between
315 FOXC2$^+$-SSCs and other SSCs subpopulations proposed previously should be revealed via
316 biological methods such as multiple lineage tracing and live imaging. Collectively, our work here
317 provides new insights into the investigation of adult SSCs and serves as a reference for studying
318 the homeostasis and regeneration of other stem-cell systems.

319
320 **Materials and Methods**
321
322 **Data Availability.** All data are available in the main text or supplementary materials. The scRNA-
323 seq and CUT&Tag sequencing data have been uploaded to the GEO with accession codes
324 GSE183163, GSE180729, and GSE180926. All of the R packages were available online and the
325 code was used according to respective R packages documentation as described in the Methods.
326 The MSigDB (v.7.0) used in this study is available at https://www.gsea-msigdb.org/gsea/msigdb.
327 **Additional Experimental Procedures.** The procedures for mice, magnetic-activated cell sorting
328 (MACS), single-cell RNA-seq, single-cell RNA-seq data processing, CUT & TAG sequencing and

analysis, enrichment analyses, transplantation assay, fluorescence-activated cell sorting (FACS), immunofluorescence, RNA isolation and quantitative RT-PCR analysis, tamoxifen inducible, analyses of cell density, sperm counts, histology, evaluation of degenerating tubules, and statistical analysis are presented in the Supplemental Materials and Methods.

**Acknowledgments**

**References**

1. S. Sharma, J. Wistuba, T. Pock, S. Schlatt, N. Neuhaus, Spermatogonial stem cells: updates from specification to clinical relevance. *Hum Reprod Update* **25**, 275-297 (2019).
2. D. G. de Rooij, L. D. Russell, All you wanted to know about spermatogonia but were afraid to ask. *J Androl* **21**, 776-798 (2000).
3. C. Huckins, Cell cycle properties of differentiating spermatogonia in adult Sprague-Dawley rats. *Cell Tissue Kinet* **4**, 139-154 (1971).
4. E. F. Oakberg, A new concept of spermatogonial stem-cell renewal in the mouse and its relationship to genetic effects. *Mutat Res* **11**, 1-7 (1971).
5. K. Hara *et al.*, Mouse spermatogenic stem cells continually interconvert between equipotent singly isolated and syncytial states. *Cell Stem Cell* **14**, 658-672 (2014).
6. A. R. Helsel *et al.*, ID4 levels dictate the stem cell state in mouse spermatogonia. *Development* **144**, 624-634 (2017).
7. G. M. Aloisio *et al.*, PAX7 expression defines germline stem cells in the adult testis. *J Clin Invest* **124**, 3929-3944 (2014).
8. M. Jijiwa *et al.*, GDNF-mediated signaling via RET tyrosine 1062 is essential for maintenance of spermatogonial stem cells. *Genes Cells* **13**, 365-374 (2008).
9. M. Sharma *et al.*, Identification of EOMES-expressing spermatogonial stem cells and their regulation by PLZF. *Elife* **8** (2019).
10. A. Sada, A. Suzuki, H. Suzuki, Y. Saga, The RNA-binding protein NANOS2 is required to maintain murine spermatogonial stem cells. *Science* **325**, 1394-1398 (2009).
11. M. Tokue *et al.*, SHISA6 Confers Resistance to Differentiation-Promoting Wnt/β-Catenin Signaling in Mouse Spermatogenic Stem Cells. *Stem Cell Reports* **8**, 561-575 (2017).
12. H. M. La *et al.*, Identification of dynamic undifferentiated cell states within the male germline. *Nat Commun* **9**, 2819 (2018).
13. J. M. Oatley, M. R. Avarbock, R. L. Brinster, Glial cell line-derived neurotrophic factor regulation of genes essential for self-renewal of mouse spermatogonial stem cells is dependent on Src family kinase signaling. *J Biol Chem* **282**, 25842-25851 (2007).
14. R. Guo *et al.*, Stage-specific and tissue-specific expression characteristics of differentially expressed genes during mouse spermatogenesis. *Mol Reprod Dev* **67**, 264-272 (2004).
15. T. Nakagawa *et al.*, A multistate stem cell dynamics maintains homeostasis in mouse spermatogenesis. *Cell Rep* **37**, 109875 (2021).

375    16.   C. T. J. van Velthoven, T. A. Rando, Stem Cell Quiescence: Dynamism, Restraint, and Cellular
376        Idling. *Cell Stem Cell* **24**, 213-225 (2019).
377    17.   J. Guo *et al.*, The adult human testis transcriptional cell atlas. *Cell Res* **28**, 1141-1157 (2018).
378    18.   B. P. Hermann *et al.*, The Mammalian Spermatogenesis Single-Cell Transcriptome, from
379        Spermatogonial Stem Cells to Spermatids. *Cell Rep* **25**, 1650-1667.e1658 (2018).
380    19.   M. Wang *et al.*, Single-Cell RNA Sequencing Analysis Reveals Sequential Cell Fate Transition
381        during Human Spermatogenesis. *Cell Stem Cell* **23**, 599-614.e594 (2018).
382    20.   K. Tan, M. F. Wilkinson, Human Spermatogonial Stem Cells Scrutinized under the Single-Cell
383        Magnifying Glass. *Cell Stem Cell* **24**, 201-203 (2019).
384    21.   S. Suzuki, J. R. McCarrey, B. P. Hermann, An mTORC1-dependent switch orchestrates the
385        transition between mouse spermatogonial stem cells and clones of progenitor spermatogonia.
386        *Cell Rep* **34**, 108752 (2021).
387    22.   H. Kubota, M. R. Avarbock, R. L. Brinster, Culture conditions and single growth factors affect
388        fate determination of mouse spermatogonial stem cells. *Biol Reprod* **71**, 722-731 (2004).
389    23.   S. S. Hammoud *et al.*, Chromatin and transcription transitions of mammalian adult germline
390        stem cells and spermatogenesis. *Cell Stem Cell* **15**, 239-253 (2014).
391    24.   M. Kanatsu-Shinohara, H. Morimoto, T. Shinohara, Enrichment of mouse spermatogonial
392        stem cells by melanoma cell adhesion molecule expression. *Biol Reprod* **87**, 139 (2012).
393    25.   F. W. Buaas *et al.*, Plzf is required in adult male germ cells for stem cell self-renewal. *Nat*
394        *Genet* **36**, 647-652 (2004).
395    26.   J. A. Costoya *et al.*, Essential role of Plzf in maintenance of spermatogonial stem cells. *Nat*
396        *Genet* **36**, 653-659 (2004).
397    27.   H. M. La, R. M. Hobbs, Mechanisms regulating mammalian spermatogenesis and fertility
398        recovery following germ cell depletion. *Cell Mol Life Sci* **76**, 4071-4102 (2019).
399    28.   T. Nakagawa, Y. Nabeshima, S. Yoshida, Functional identification of the actual and potential
400        stem cell compartments in mouse spermatogenesis. *Dev Cell* **12**, 195-206 (2007).
401    29.   Y. Clermont, Renewal of spermatogonia in man. *Am J Anat* **118**, 509-524 (1966).
402    30.   Y. Clermont, Spermatogenesis in man. A study of the spermatogonial population. *Fertil Steril*
403        **17**, 705-721 (1966).
404    31.   Y. Clermont, Two classes of spermatogonial stem cells in the monkey (Cercopithecus
405        aethiops). *Am J Anat* **126**, 57-71 (1969).
406    32.   J. Ehmcke, S. Schlatt, A revised model for spermatogonial expansion in man: lessons from
407        non-human primates. *Reproduction* **132**, 673-680 (2006).
408    33.   J. Ehmcke, J. Wistuba, S. Schlatt, Spermatogonial stem cells: questions, models and
409        perspectives. *Hum Reprod Update* **12**, 275-282 (2006).
410    34.   D. Wang *et al.*, Identification of multipotent mammary stem cells by protein C receptor
411        expression. *Nature* **517**, 81-84 (2015).
412    35.   K. Zheng, X. Wu, K. H. Kaestner, P. J. Wang, The pluripotency factor LIN28 marks
413        undifferentiated spermatogonia in mouse. *BMC Dev Biol* **9**, 38 (2009).
414    36.   Y. Toyooka *et al.*, Expression and intracellular localization of mouse Vasa-homologue protein
415        during germ cell development. *Mech Dev* **93**, 139-149 (2000).
416    37.   H. Li *et al.*, DAZL is a master translational regulator of murine spermatogenesis. *Natl Sci Rev*
417        **6**, 455-468 (2019).
418    38.   T. Gallardo, L. Shirley, G. B. John, D. H. Castrillon, Generation of a germ cell-specific mouse
419        transgenic Cre line, Vasa-Cre. *Genesis* **45**, 413-417 (2007).
420    39.   H. S. Kaya-Okur, D. H. Janssens, J. G. Henikoff, K. Ahmad, S. Henikoff, Efficient low-cost
421        chromatin profiling with CUT&Tag. *Nat Protoc* **15**, 3264-3283 (2020).

422  40.  H. S. Kaya-Okur *et al.*, CUT&Tag for efficient epigenomic profiling of small samples and single
423       cells. *Nat Commun* **10**, 1930 (2019).
424  41.  R. Bahar *et al.*, Growth retardation, polyploidy, and multinucleation induced by Clast3, a novel
425       cell cycle-regulated protein. *J Biol Chem* **277**, 40012-40019 (2002).
426  42.  C. M. Knudson, S. J. Korsmeyer, Bcl-2 and Bax function independently to regulate cell death.
427       *Nat Genet* **16**, 358-363 (1997).
428  43.  M. van Oosten *et al.*, Mismatch repair protein Msh2 contributes to UVB-induced cell cycle
429       arrest in epidermal and cultured mouse keratinocytes. *DNA Repair (Amst)* **4**, 81-89 (2005).
430  44.  J. L. Nitiss, DNA topoisomerase II and its growing repertoire of biological functions. *Nat Rev
431       Cancer* **9**, 327-337 (2009).
432  45.  X. Yi *et al.*, RNA processing and modification protein, carbon catabolite repression 4 (Ccr4),
433       arrests the cell cycle through p21-dependent and p53-independent pathway. *J Biol Chem* **287**,
434       21045-21057 (2012).
435  46.  P. Gaudet, M. S. Livstone, S. E. Lewis, P. D. Thomas, Phylogenetic-based propagation of
436       functional annotations within the Gene Ontology consortium. *Brief Bioinform* **12**, 449-462
437       (2011).
438  47.  B. A. Weaver *et al.*, Centromere-associated protein-E is essential for the mammalian mitotic
439       checkpoint to prevent aneuploidy due to single chromosome loss. *J Cell Biol* **162**, 551-563
440       (2003).
441  48.  M. M. Georgescu, G. Cote, N. K. Agarwal, C. L. White, 3rd, NHERF1/EBP50 controls
442       morphogenesis of 3D colonic glands by stabilizing PTEN and ezrin-radixin-moesin proteins at
443       the apical membrane. *Neoplasia* **16**, 365-374.e361-362 (2014).
444  49.  M. Raman, S. Earnest, K. Zhang, Y. Zhao, M. H. Cobb, TAO kinases mediate activation of
445       p38 in response to DNA damage. *Embo j* **26**, 2005-2014 (2007).
446  50.  W. J. Bakker *et al.*, FoxO3a regulates erythroid differentiation and induces BTG1, an activator
447       of protein arginine methyl transferase 1. *J Cell Biol* **164**, 175-184 (2004).
448  51.  K. E. Davis, M. Moldes, S. R. Farmer, The forkhead transcription factor FoxC2 inhibits white
449       adipocyte differentiation. *J Biol Chem* **279**, 42453-42461 (2004).
450  52.  A. Sabine *et al.*, FOXC2 and fluid shear stress stabilize postnatal lymphatic vasculature. *J Clin
451       Invest* **125**, 3861-3877 (2015).
452  53.  F. Arai, T. Suda, Maintenance of quiescent hematopoietic stem cells in the osteoblastic niche.
453       *Ann N Y Acad Sci* **1106**, 41-53 (2007).
454  54.  F. Relaix, P. S. Zammit, Satellite cells are essential for skeletal muscle regeneration: the cell
455       on the edge returns centre stage. *Development* **139**, 2845-2856 (2012).
456  55.  J. T. Rodgers *et al.*, mTORC1 controls the adaptive transition of quiescent stem cells from G0
457       to G(Alert). *Nature* **510**, 393-396 (2014).
458  56.  C. Wei, H. Lin, S. Cui, The Forkhead Transcription Factor FOXC2 Is Required for Maintaining
459       Murine Spermatogonial Stem Cells. *Stem Cells Dev* **27**, 624-636 (2018).
460  57.  N. Miura, K. Iida, H. Kakinuma, X. L. Yang, T. Sugiyama, Isolation of the mouse (MFH-1) and
461       human (FKHL 14) mesenchyme fork head-1 genes reveals conservation of their gene and
462       protein structures. *Genomics* **41**, 489-492 (1997).

## Figures and Tables
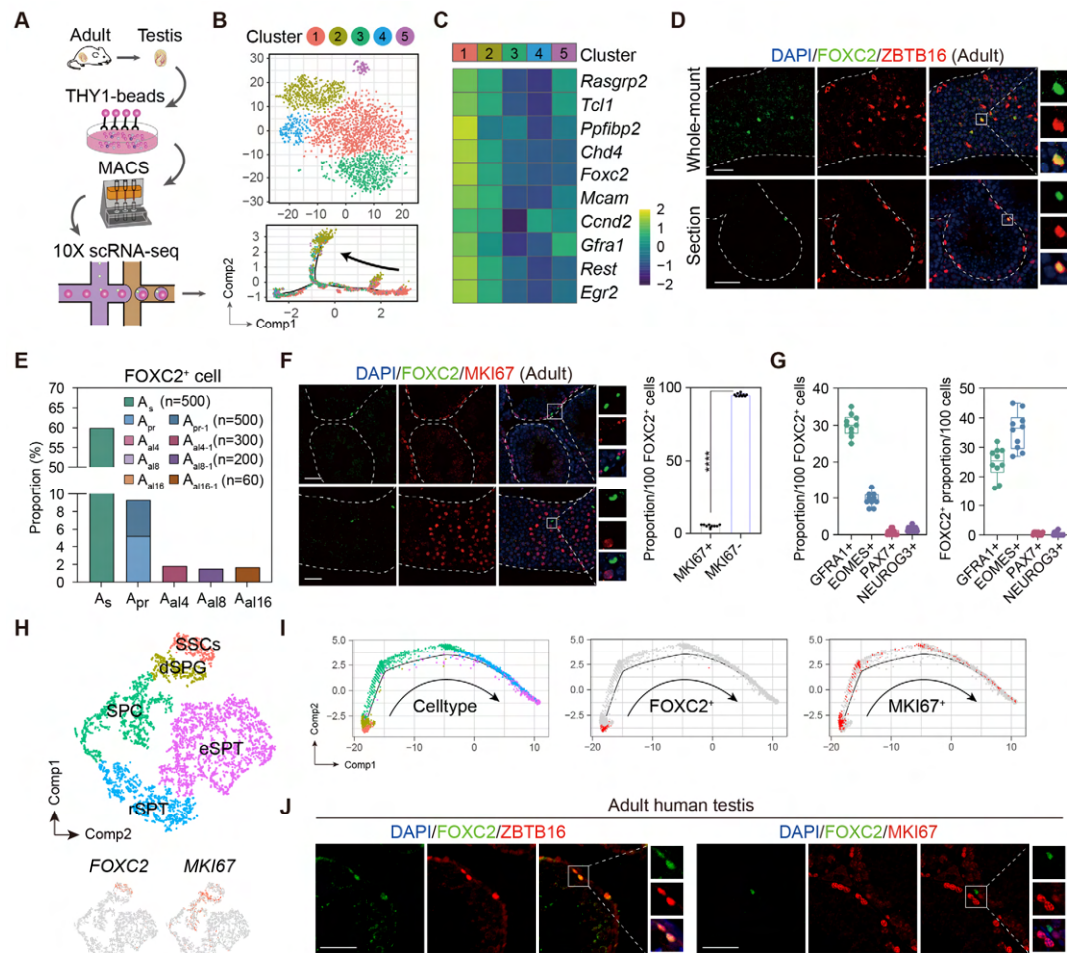


**Figure 1. Identification of the FOXC2$^+$-SSCs in adult mouse and human testis.** (**A**) Schematic illustration of the single-cell analysis workflow. (**B**) t-SNE plot and developmental trajectory of all uSPG, colored by cluster. (**C**) Heatmap of the Top10 DEGs in Cluster1. (**D**) Immunostaining for ZBTB16 (red), FOXC2 (green), and DAPI (blue) in testicular paraffin sections from wild-type adult C57 mice. Scale bar, 50 μm; C57, C57BL/6J. (**E**) The proportion of FOXC2$^+$ cells in different uSPG subtypes. (**F**) Immunostainings for MKI67 (red), FOXC2 (green), and DAPI (blue) in adult mice testis and the proportion of MKI67$^+$ cells in FOXC2$^+$ population (n=10). Scale bar, 50 μm; values, mean ± s.e.m.; p-values were obtained using two-tailed t-tests (****p-value < 0.0001). (**G**) The co-expression proportion between the FOXC2 and differential known SSCs makers (n=10). (**H**) t-SNE plot of germ cells in adult human testis (GSE112013), colored by germ cell type. Feature plot showing the expression patterns of *FOXC2* and *MKI67* in human germ cells. (**I**) The developmental trajectory of the human germ cells, colored by germ cell type, FOXC2 expression cells (red), or MKI67 expression cells (red). (**J**) Immunostaining for ZBTB16/MKI67 (red), FOXC2 (green), and DAPI (blue) in testicular paraffin sections from adult humans.
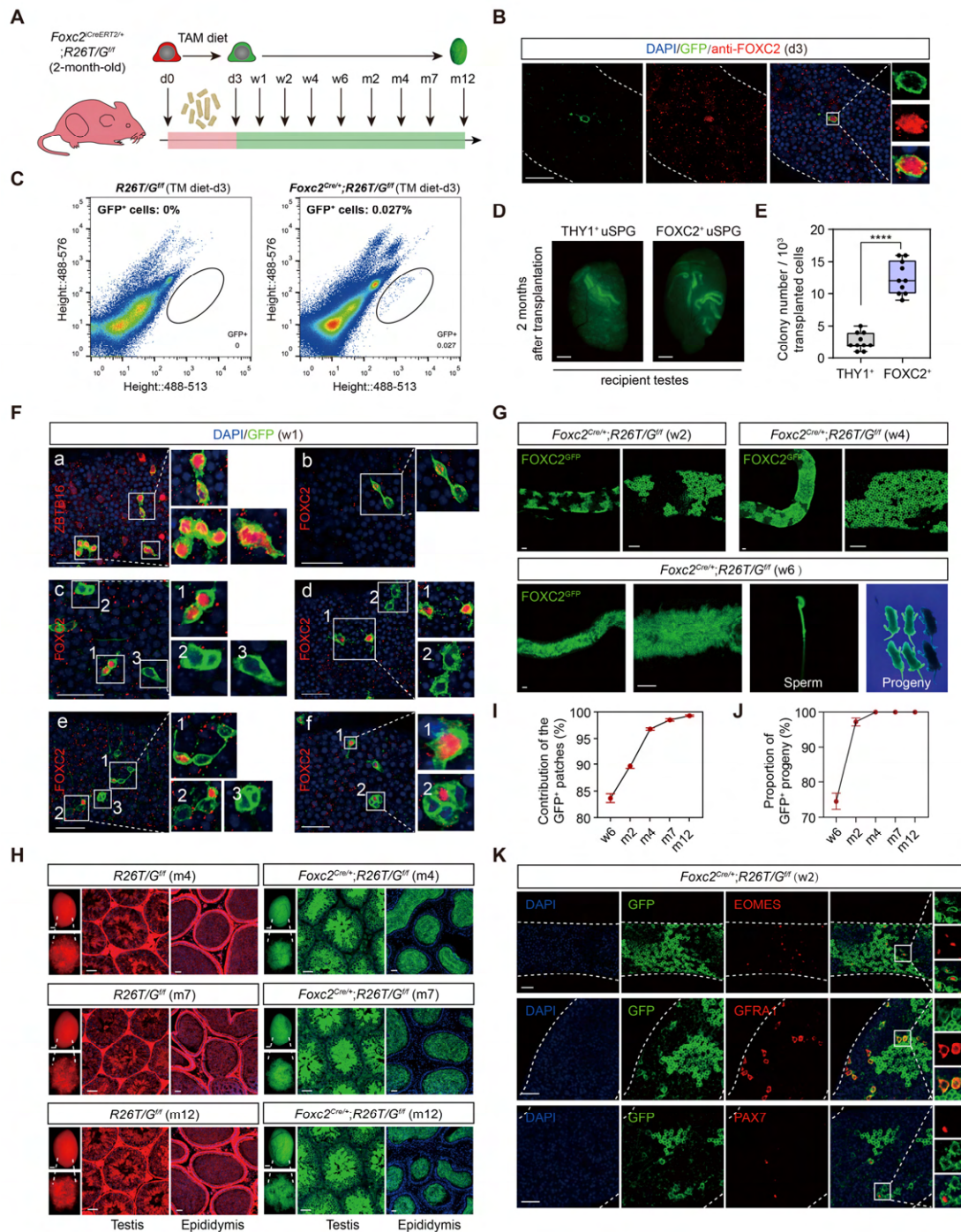
481
482
**Figure 2. Lineage tracing and functional validation of FOXC2$^+$-SSCs in *Foxc2$^{CRE/+}$*;*R26T/G$^{f/f}$***
**mice.** (**A**) Schematic illustration of the lineage tracing workflow for FOXC2$^+$ cells. (**B**)
Immunostainings for DAPI (blue) and FOXC2 (red) at day 3 post TAM induction. Scale bar, 50 μm;
d, day. (**C**) FACS analysis of GFP$^+$ populations derived from *R26T/G$^{f/f}$* or *Foxc2$^{CRE/+}$*;*R26T/G$^{f/f}$* mice
at day 3 post TAM induction. (**D**, **E**) The recipient mice testes (**D**) and colony numbers (**E**) 2 months

488   after transplantation (n=10) of the FACS-sorted GFP$^+$ cells from the *Foxc2$^{CRE/+}$;R26T/G$^{f/f}$* mice 3
489   days after TAM diet and the MACS-sorted THY1$^+$ cells from adult mice. Scale bar, 1 mm; values,
490   mean ± s.e.m.; p-values were obtained using two-tailed t-tests (****p-value < 0.0001). (**F**)
491   Immunostaining for DAPI (blue), ZBTB16/FOXC2 (red), and GFP (green) at week 1 post TAM
492   induction (scale bar, 50 µm). (**G**) Seminiferous tubules of *Foxc2$^{CRE/+}$;R26T/G$^{f/f}$* mice 2, 4, and 6
493   weeks post TAM induction. Scale bar, 50 µm. (**H**) Testes (scale bar, 1 mm), seminiferous tubules,
494   and epididymis (scale bar, 50 µm) at month 4, 7, and 12 post TAM induction in *Foxc2$^{CRE/+}$;R26T/G$^{f/f}$*
495   mice. (**I**, **J**) The GFP$^+$ patches (**I**) and progeny (**J**) population dynamics (n=10). Values, mean ±
496   s.e.m. (**K**) Immunostainings for DAPI (blue), EOMES (red), GFRA1 (red), or PAX7 (red) in GFP$^+$
497   population at week 2 post TAM induction. Scale bar, 50 µm.
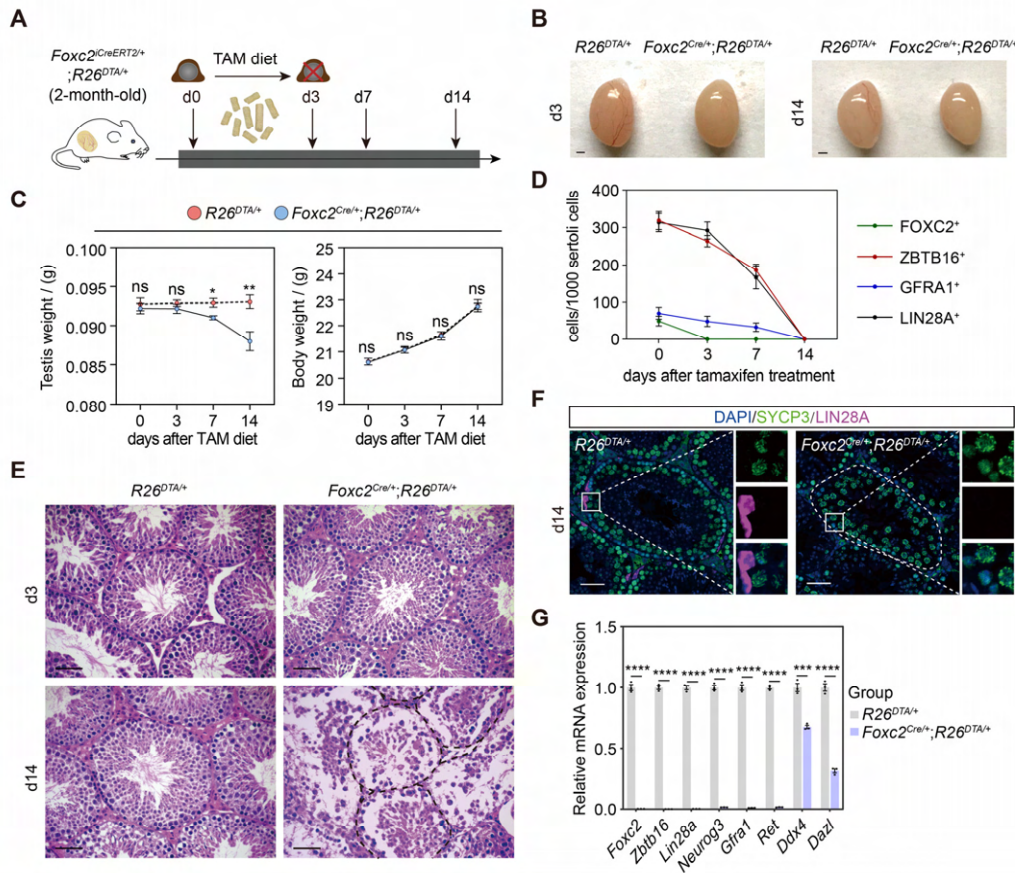
498
499
**Figure 3. Specific ablation of FOXC2$^+$-SSCs and phenotypic validation in *Foxc2$^{Cre/+}$;R26$^{DTA/+}$* mice.** (**A**) Schematic illustration of the lineage tracing workflow for FOXC2$^+$ cells. (**B-D**) Phenotypic validation of the *R26$^{DTA/+}$* and *Foxc2$^{Cre/+}$;R26$^{DTA/+}$* mice (n=5) for testes size (**B**), testis weight and body weight (**C**), and HE-staining of the testes (**D**). Scale bars in (**B**), 1 mm; in (**D**), 50 μm; d, day; values were mean ± s.e.m.; p-values were obtained using two-tailed t-tests (ns > 0.05, *p-value < 0.05, **p-value < 0.01). (**E**) ZBTB16$^+$, GFRA1$^+$, LIN28A$^+$, and FOXC2$^+$ SPG populations dynamics. Values, mean ± s.e.m. (n=10); p-values were obtained using one-way ANOVA followed by Tuke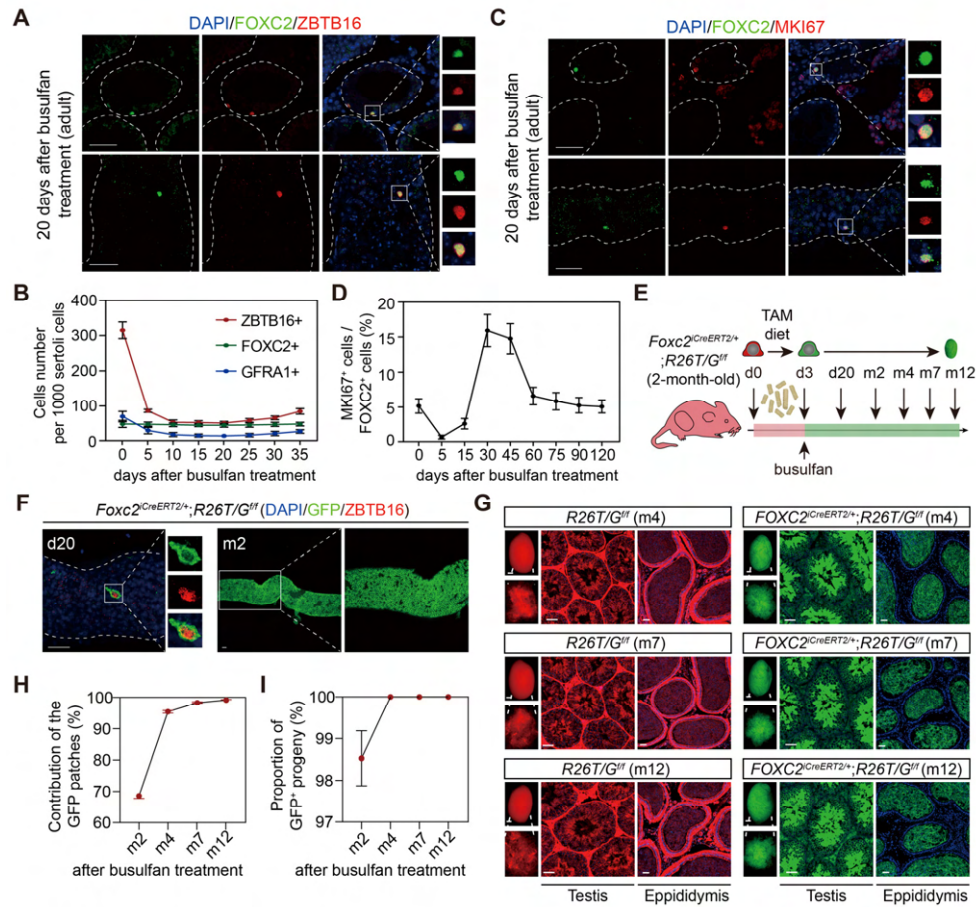y test (ns > 0.05, *p-value < 0.05, **p-value < 0.01, ****p-value < 0.0001). (**F**) Immunostainings for DAPI (blue), SYCP3 (green), and LIN28A (magenta) at day 14 post TAM induction. d, day; scale bar, 50 μm. (**G**) Quantitative RT-PCR analysis of SPG markers expression in the testes of the *R26$^{DTA/+}$* and *Foxc2$^{Cre/+}$;R26$^{DTA/+}$* mice (n=3). Values, mean ± s.e.m.; p-values were obtained using two-tailed t-tests (***p-value < 0.001, ****p-value < 0.0001).

**Figure 4. FOXC2⁺-SSCs are critical for germline regeneration.** (**A**) Co-immunostaining of FOXC2 (green) with ZBTB16 (red) in seminiferous tubules of the adult testes at day 20 post busulfan treatment. Scale bar, 50 μm. (**B**) ZBTB16⁺, GFRA1⁺, and FOXC2⁺ population dynamics after busulfan treatment (20 mg/kg, n=10). (**C**) Co-immunostaining of FOXC2 (green) with MKI67 (red) in seminiferous tubules of the adult testes at day 20 post busulfan treatment. Scale bar, 50 μm. (**D**) MKI67⁺FOXC2⁺ proportions in relation to the whole FOXC2⁺ population at different time points after busulfan treatment (n=4). (**E**) Schematic illustration for lineage tracing of FOXC2⁺ cell after busulfan treatment. (**F**) Lineage tracing of the GFP⁺ cells at day 20 and month 2 after busulfan treatment (scale bar, 50 μm). (**G**) The testes (scale bar, 1 mm), seminiferous tubules, and epididymis (scale bar, 50 μm) at month 4, 7, and 12 post TAM induction and busulfan injection. m, month. (**H**, **I**) The proportion dynamics of GFP patches (**H**) and GFP⁺ progenies (**I**). Values, mean ± s.e.m. (n=10). w, week; m, month.
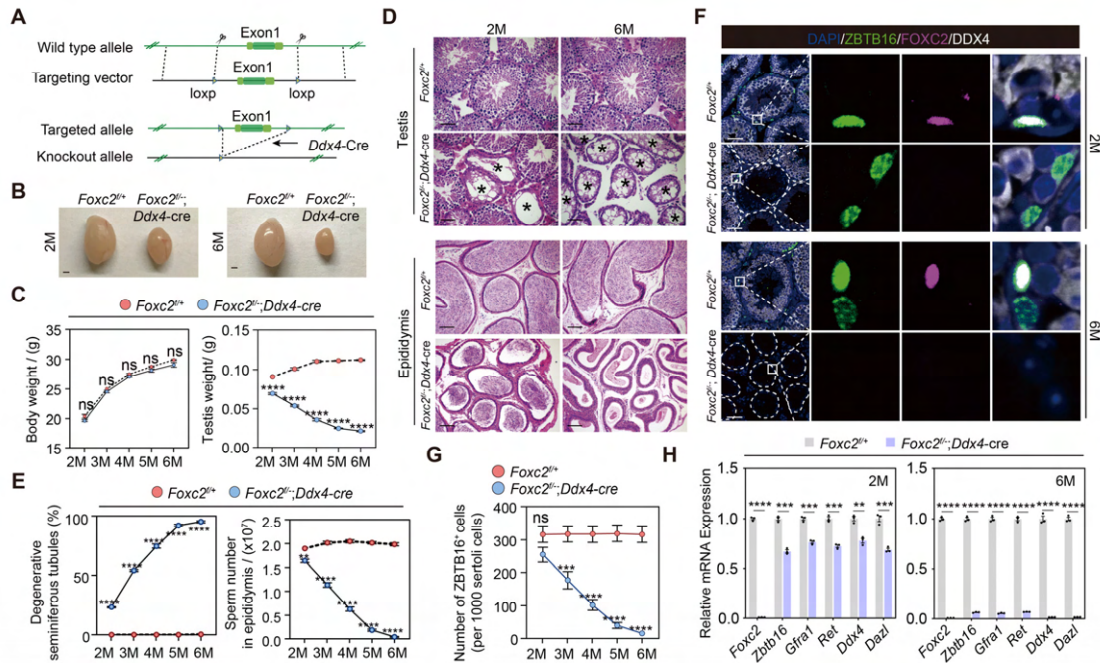
**Figure 5. Spermatogenesis exhaustion in the adult *Foxc2^{f/-};Ddx4*-cre mice.** (**A**) Construction of the *Foxc2^{f/-};Ddx4*-cre mice. (**B**) The testes size of the *Foxc2^{f/-};Ddx4*-cre mice. Scale bar, 1mm; M, month. (**C**) Body weight and testis weight of the *Foxc2^{f/-};Ddx4*-cre mice at different age (n=5). M, month; values, mean ± s.e.m.; p-values were obtained using two-tailed t-tests (ns > 0.05, ****p-value < 0.0001). (**D**) HE-staining of the testis and epididymis. Scale bar, 50 μm; M, month. (**E**) Estimation of degenerative tubules and sperm counts in cauda epididymis of the *Foxc2^{f/+}* and *Foxc2^{f/-};Ddx4*-cre mice with age (n=5). Values, mean ± s.e.m.; p-values were obtained using two-tailed t-tests (**p-value < 0.01, ****p-value < 0.0001). (**F**) Immunostainings for DAPI (blue), ZBTB16 (green), FOXC2 (magenta), and DDX4 (white) in the seminiferous tubules of the *Foxc2^{f/+}* and *Foxc2^{f/-}; Ddx4*-cre mice. Scale bar, 50 μm. (**G**) Estimation of ZBTB16^+ uSPG number in the *Foxc2^{f/+}* and *Foxc2^{f/-};Ddx4*-cre mice with age (n=5). Values, mean ± s.e.m.; p-values were obtained using two-tailed t-tests (ns > 0.05, ***p-value < 0.001, ****p-value < 0.0001). (**H**) Quantitative RT-PCR analysis of the uSPG and germ cell markers expressed in the testis of the *Foxc2^{f/+}* and *Foxc2^{f/-}; Ddx4*-cre mice (n=3). M, month; values, mean ± s.e.m.; p-values were obtained using two-tailed t-tests (**p-value < 0.01, ***p-value < 0.001, ****p-value < 0.0001).

17
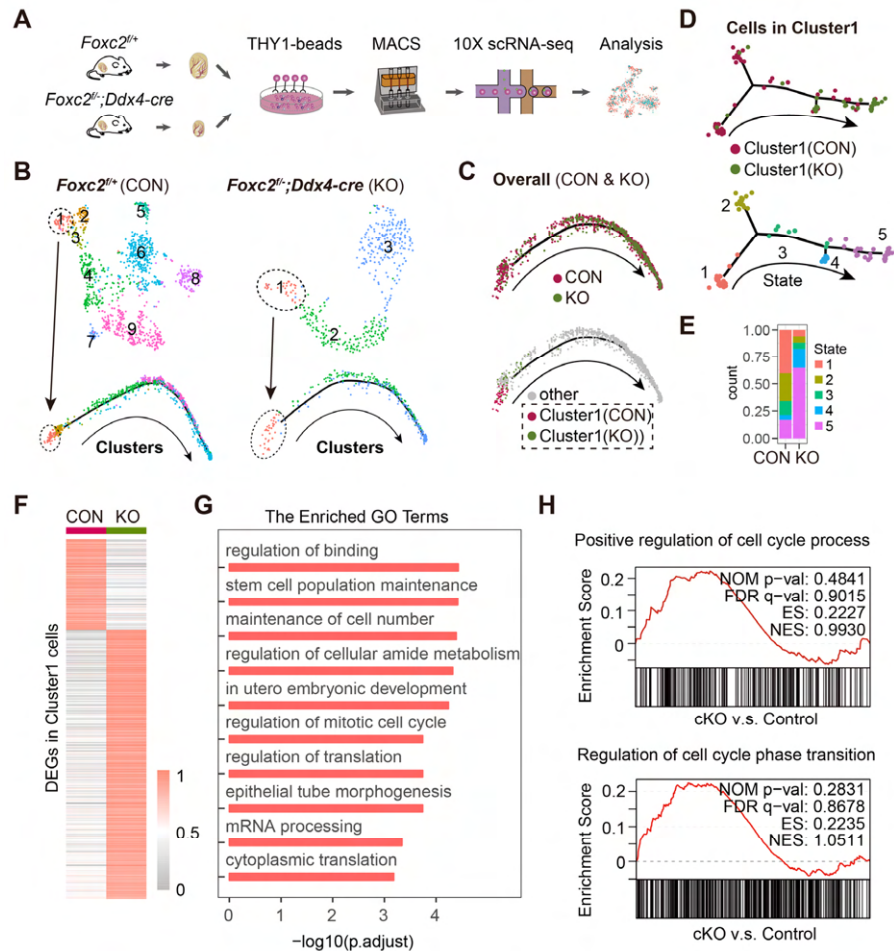
**Figure 6. scRNA-seq analysis of THY1$^+$ uSPG in *Foxc2$^{f/+}$* and *Foxc2$^{f/-}$;Ddx4*-cre mice.** (**A**) Schematic illustration of the scRNA-seq workflow. (**B**) t-SNE plot and developmental trajectory of uSPG from *Foxc2$^{f/+}$* and *Foxc2$^{f/-}$;Ddx4*-cre mice respectively, colored by cluster. (**C**) Developmental trajectories of uSPG from *Foxc2$^{f/+}$* and *Foxc2$^{f/-}$;Ddx4*-cre mice, colored by sample or derivation. (**D**) Developmental trajectories of the cells in Cluster1 from *Foxc2$^{f/+}$* (CON) and *Foxc2$^{f/-}$;Ddx4*-cre (KO) mice, colored by derivation or developmental state. (**E**) The Cluster1 cells proportion of each state in CON and KO mice. (**F**) Heatmap showing the DEGs in the Cluster1 cells from the *Foxc2$^{f/-}$;Ddx4*-cre mice compared with the *Foxc2$^{f/+}$* mice. (**G**) Top GO terms enrichment by the down-regulated DEGs in KO mice. (**H**) Gene set enrichment analysis (GSEA) of the Cluster1 cells (*Foxc2$^{f/-}$;Ddx4*-cre v.s. *Foxc2$^{f/+}$* mice). NOM, nominal; FDR, false discovery rate; ES, enrichment score; NES, normalized enrichment score.
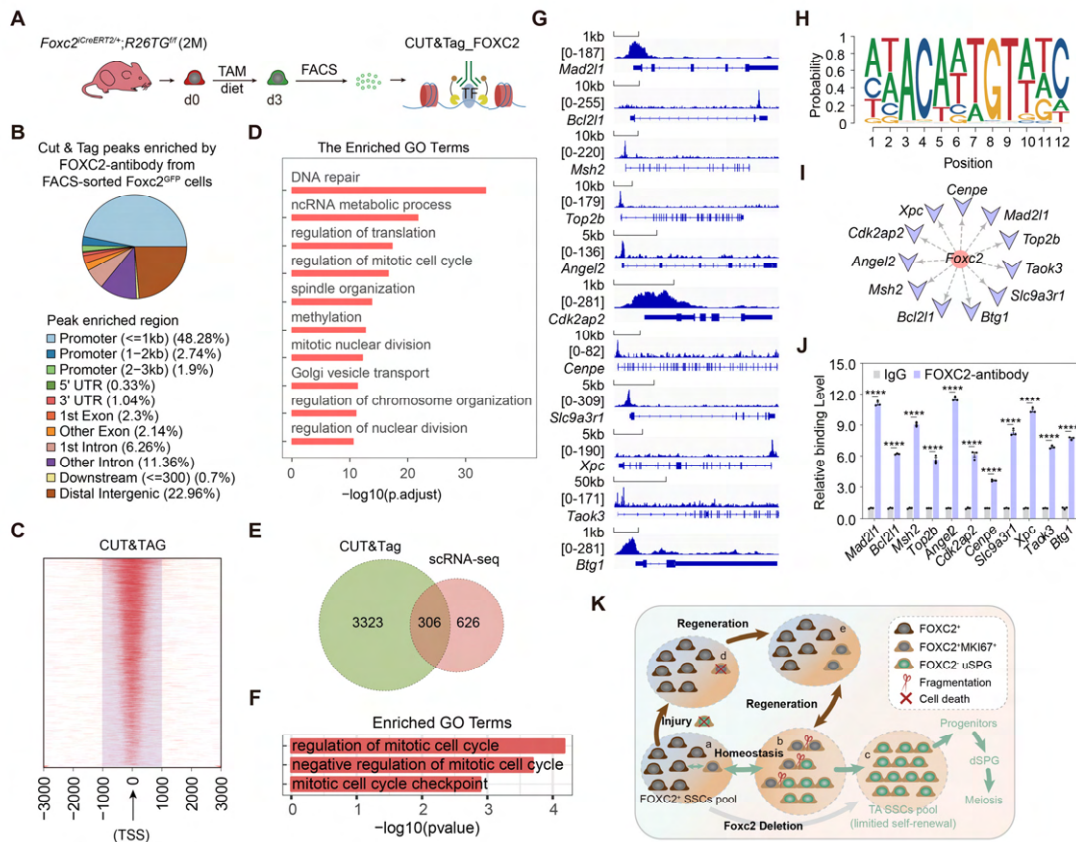
**Figure 7. FOXC2 is essential for sustaining the primitive SSCs via regulating cell cycle.** (**A**) Workflow schematic illustration of the CUT&Tag_FOXC2 analysis on the FACS-sorted FOXC2+ cells. (**B**) Pie chart for CUT&Tag_FOXC2 peaks genome distribution. (**C**) Profiling of CUT&Tag_FOXC2 peaks in proximity to transcriptional starting site (TSS). The distance to TSS within 1000 was highlighted in the purple box. (**D**) Top GO terms enrichment by genes annotated by CUT&Tag_FOXC2 peaks. (**E**) Venn diagram of FOXC2 target genes defined by overlapping the CUT&Tag sequencing and scRNA-seq datasets. (**F**) GO terms enrichment by the FOXC2 target genes related to cell cycle regulation. (**G**) Chromatin landscapes of CUT&Tag_FOXC2 peaks of the candidates associated with negative cell cycle regulation. (**H**) The DNA-binding motif for FOXC2 (predicted with HOMER). (**I**) The cell cycle-related candidates possessing high binding potential (>0.8, predicted with JASPAR SCAN). (**J**) CUT&Tag-qPCR validation of the cell cycle arrest regulatory genes. (n=3). Values, mean ± s.e.m.; p-values were obtained using two-tailed t-tests (****p-value < 0.0001). (**K**) The model for the maintenance of the FOXC2+ SSCs subpopulation in adult testis.

19

572 **Supplemental Figures**

573



574
575
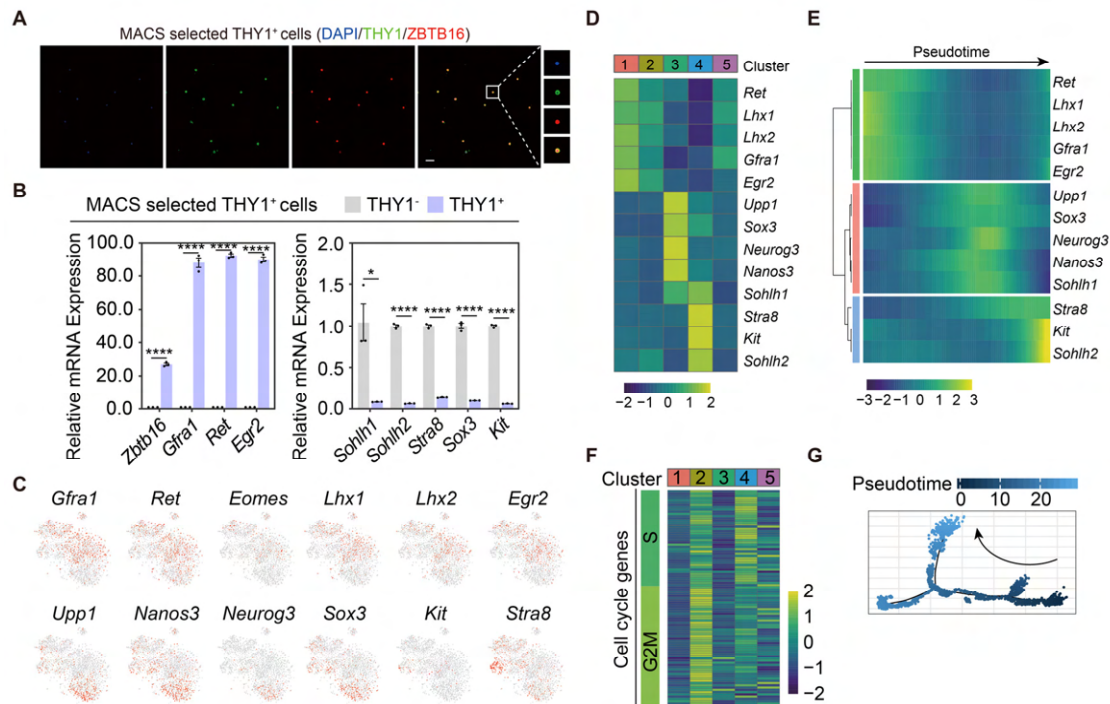
576 **Figure S1. Validation and characterization of the MACS-sorted THY1$^+$ uSPG from wild-type**
577 **adult C57 mice.** (**A**) Immunostainings of DAPI (blue), THY1 (green), and ZBTB16 (red) in the
578 MACS-sorted THY1$^+$ cells (n=5). Scale bar, 50 µm. (**B**) Quantitative RT-PCR analysis of uSPG and
579 dSPG markers expressed in the MACS-sorted THY1$^+$ cells (n=3). Values, mean ± s.e.m.; p-values
580 were obtained using two-tailed t-tests (ns > 0.05, *p-value < 0.05, **p-value < 0.01, ***p-value <
581 0.001, ****p-value < 0.0001). (**C**) Feature plots showing the expression pattern of classic SPG
582 markers (stemness and differentiation). (**D**) Heatmap showing the expression pattern of markers
583 for SPG in different clusters. (**E**) Expression pattern dynamics of the SPG markers with pseudotime
584 progression. (**F**) Heatmap showing the expression pattern of markers for cell cycle phase in
585 different clusters. (**G**) The developmental trajectory of the overall SPG, colored by pseudotime.
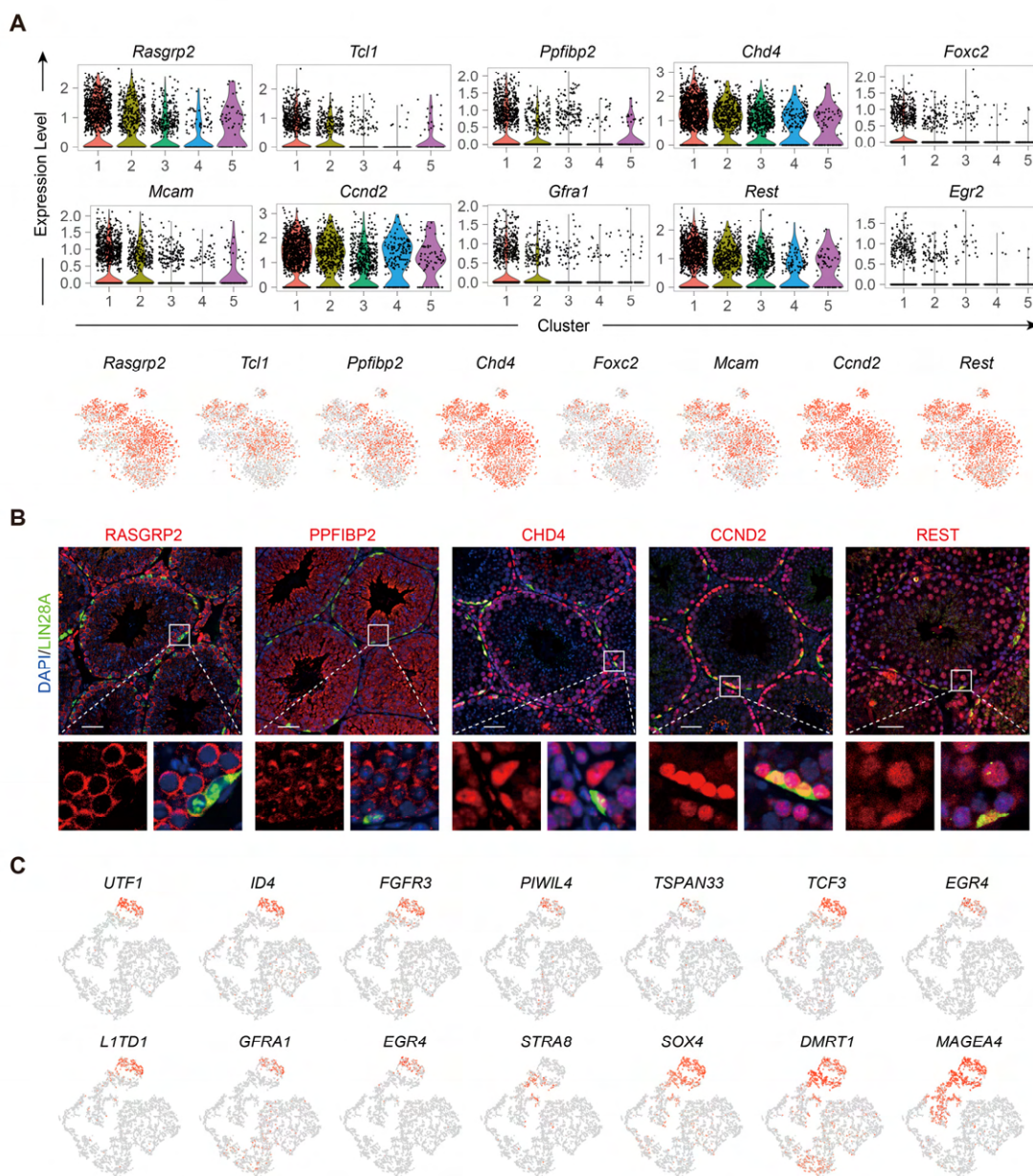
**Figure S2. Expression of top10 DEGs of Cluster1 in Figure 1B and classic SSC and SPG markers in adult human germ cells.** (**A**) Feature plots and violin plots of the Top10 DEGs of Cluster1. (**B**) Immunostainings for LIN28A (red), DAPI (blue), and newly-found markers (green) in testicular paraffin sections from adult mice. Scale bar, 50 μm. (**C**) Feature plots showing the expression pattern of classic SSCs and SPG markers in adult human germ cells.
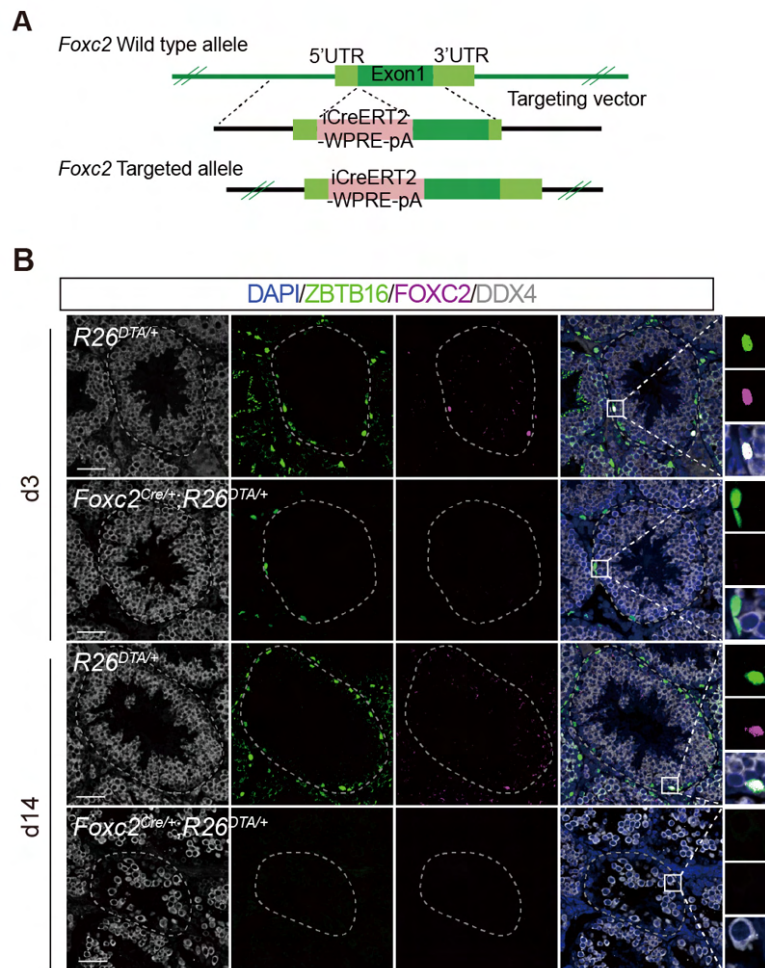
593
594
595 **Figure S3. Construction of the *Foxc2^iCreERt2* mice and depletion of uSPG pool in**
596 ***Foxc2^Cre/+;R26^DTA/+* mice 14 days after specific ablation of FOXC2^+-SSCs.** (**A**) Construction of
597 the *Foxc2^iCreERt2* mice. (**B**) Immunostainings for DAPI (blue), DDX4 (white), ZBTB16 (green), and
598 FOXC2 (magenta) at day 3 and day 14 post TAM induction in *Foxc2^Cre/+;R26^DTA/+* mice (scale bar,
599 50 μm).
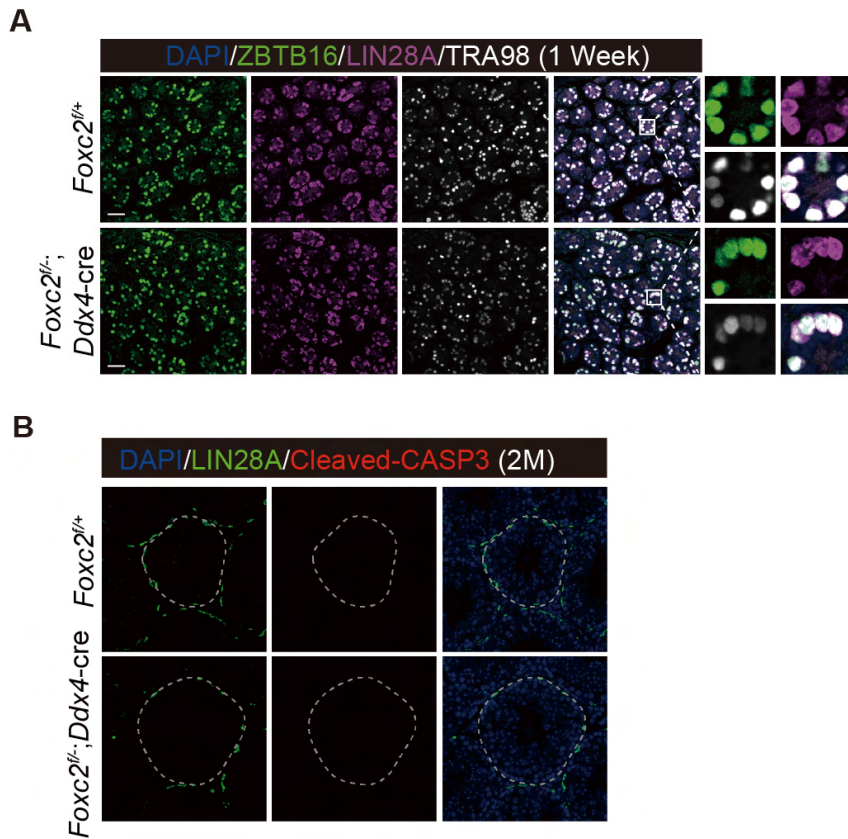
600
601
**Figure S4. Phenotypic validation of the *Foxc2^{f/-};Ddx4*-cre mice.** (**A**) Immunostainings for DAPI (blue), ZBTB16 (green), LIN28A (magenta), and TRA98 (white) in seminiferous tubules of 1-week-old *Foxc2^{f/+}* and *Foxc2^{f/-};Ddx4*-cre mice. Scale bar, 50 µm. (**B**) Immunostainings for DAPI (blue), LIN28A (green), and Cleaved-CASP3 (red) in seminiferous of the *Foxc2^{f/+}* and *Foxc2^{f/-};Ddx4*-cre mice (2-month-old). M, month; scale bar, 50 µm.
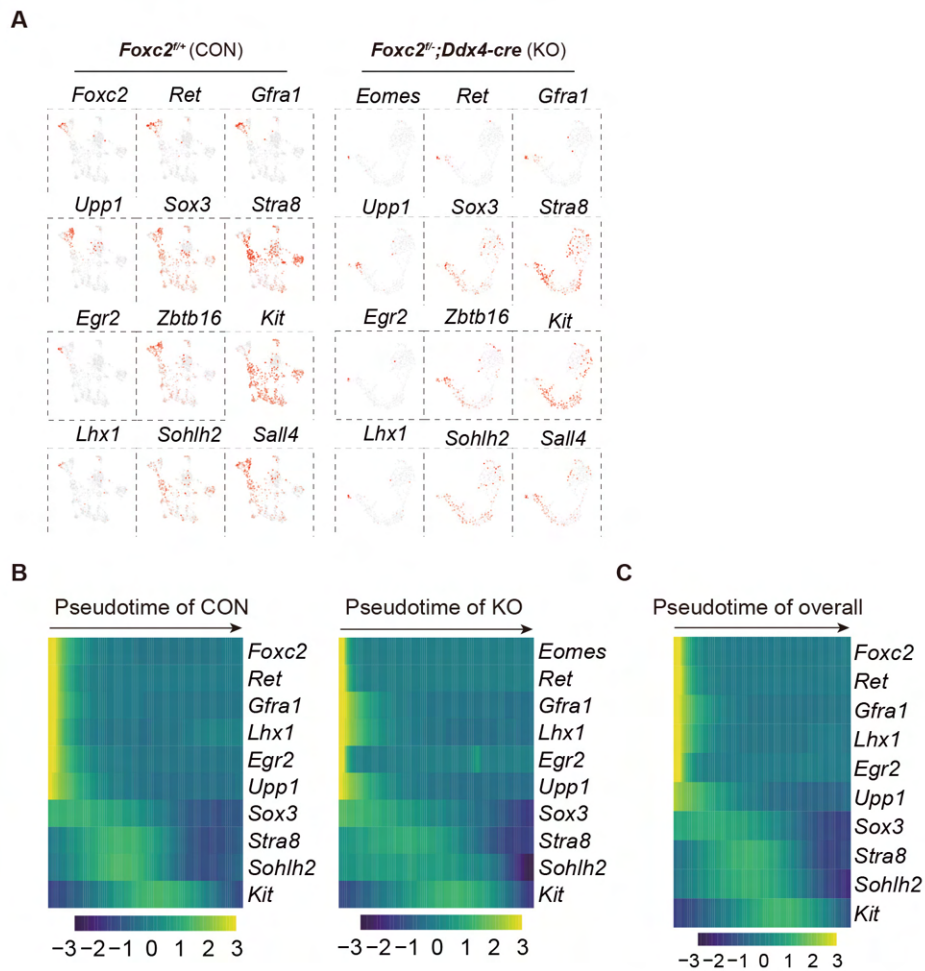
**Figure S5. scRNA-seq analysis of THY1⁺ uSPG in adult *Foxc2^{f/+}* and *Foxc2^{f/-};Ddx4*-cre mice.**
(**A**) Feature plots of classic SPG markers for uSPG in adult *Foxc2^{f/+}* or *Foxc2^{f/-};Ddx4*-cre mice. (**B**) Expression dynamics of SPG markers with pseudotime progression for uSPG from *Foxc2^{f/+}* or *Foxc2^{f/-};Ddx4*-cre mice respectively. (**C**) Expression dynamics of SPG markers with pseudotime progression for overall uSPG from *Foxc2^{f/+}* and *Foxc2^{f/-};Ddx4*-cre mice.
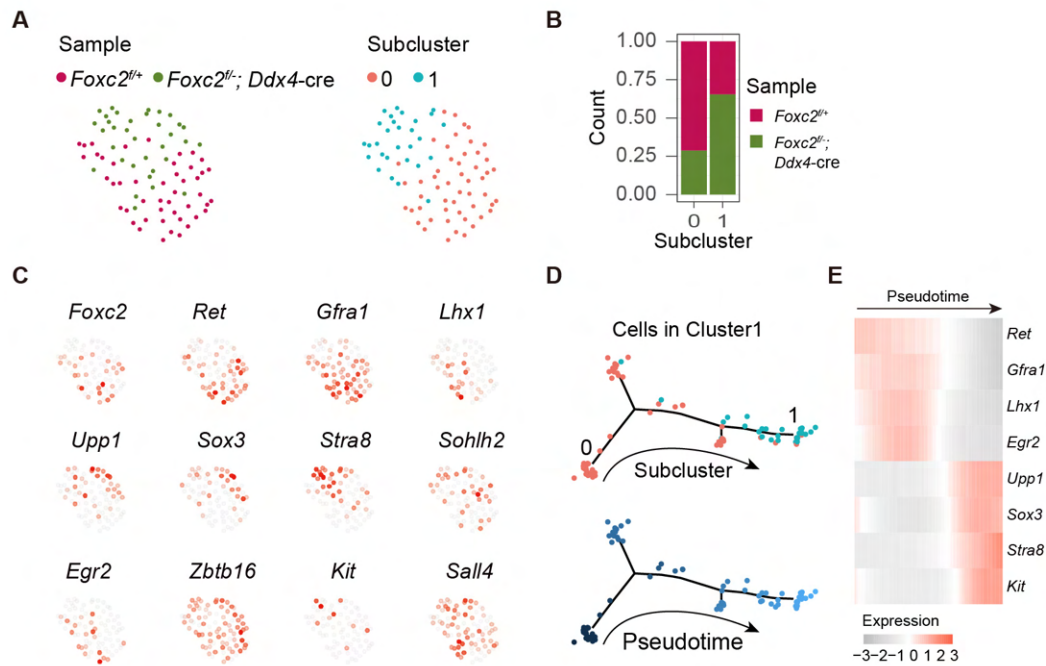
**Figure S6. Re-cluster and developmental trajectory analysis of cells in Cluster1 derived from adult *Foxc2^{f/+}* and *Foxc2^{f/-}*;*Ddx4*-cre mice.** (**A**) The t-SNE plot of the Cluster1 cells aggregated from the *Foxc2^{f/+}* and *Foxc2^{f/-}*;*Ddx4*-cre mice colored by sample or subcluster. (**B**) The cell proportion of each sample in each subcluster. (**C**) Feature plots of SPG markers expression. (**D**) Developmental trajectory of the aggregated Cluster1 cells colored by subcluster or pseudotime. (**E**) Expression dynamics of SPG markers with pseudotime progression.

622   **Supplemental Tables (separate files)**

623

624   **Supplemental Table S1**. List of the top30 differentially expressed genes of different clusters.

625   **Supplemental Table S2**. List of the differentially expressed genes found by CUT&Tag sequencing

626   and scRNA-seq respectively and their respective enriched Gene Ontology terms.

627   **Supplemental Table S3**. List of the Gene Ontology terms of the 306 crossed candidates.

628   **Supplemental Table S4**. Primers and antibodies used in this study.

629 **Supplemental Materials and Methods**
630
631 **Mice**
632 Animal experiments were approved by the Committee on Animal Care of the Institute of Basic
633 Medical Sciences, Chinese Academy of Medical Sciences and Peking Union Medical College. The
634 8-week-old C57BL/6J wild-type mice were used for magnetic-activated cell sorting. The
635 Rosa26mTmG$^{flox}$ mice (stock no. 007676), *Ddx4*-Cre mice (stock no. 000692) and EGFP$^{Tg/+}$ mice
636 (stock no. 021930) were bought from the Jackson Laboratory. The *Foxc2$^{iCreERt2}$* mice and the
637 *Foxc2$^{flox/flox}$* (*Foxc2$^{f/f}$*) mice were constructed and bought from the Biocytogen. The Rosa-eGFP-
638 DTA (R26$^{DTA}$/+) mice were bought from GemPharmatech. All mice were housed and bred under
639 specific pathogen-free conditions (temperature: 22-26°C, humidity: 40-55%, 12-h light/dark cycle)
640 in the animal facility at the Institute of Basic Medical Sciences. DNA was isolated from the tails, and
641 the genotypes of the mice were checked using PCR with specific primers (Supplemental Table S4).
642 All mice were randomly assigned to experiments and no statistical methods were used to
643 predetermine sample size. The person performing the experiments did not know the sample identity
644 until after data analysis. No data were excluded from analyses and the data displayed included a
645 minimum of three independent experiments and a minimum of three biological replicates for each
646 independent experiment. The 8-week-old C57BL/6J WT mice were treated with busulfan (40
647 mg/kg) and used as recipient mice 1 month later.
648
649 **Magnetic-activated cell sorting (MACS)**
650 The testes from 8-week-old C57BL/6J wild-type mice or 4-month-old *Foxc2$^{f/+}$* and *Foxc2$^{f/-}$*; *Ddx4-*
651 cre mice (n=4) were minced and digested in the collagenase type IV (1mg/mL, Sigma) and DNase
652 I (500μg/mL, Sigma) at 37°C for 15 min. The cell suspension was pipetted up and down once every
653 5 minutes and the digestion process was stopped with DMEM (containing 10% FBS). The cell
654 suspension was filtered through a 40-μm nylon mesh, and after centrifugation, the cells were
655 resuspended in 8mL PBS. The 15 mL conical centrifuge tubes were slowly overlaid with 2 mL of
656 70% Percoll solution, 2 mL of 30% Percoll solution, and then 2 mL of testicular cell suspension and
657 centrifuge at 600 × g for 10 min at 4 °C without using the centrifuge brake. After centrifugation, the
658 cells at the interface between the 70% and the 30% Percoll solution were carefully removed into
659 the new conical centrifuge tubes, washed with PBS, and then centrifuge at 600 × g for 10 min at
660 4 °C. After centrifugation, the cells were resuspended in 360μL MACS buffer, added with 40μL of
661 magnetic microbeads conjugated with anti-Thy-1 antibody (Miltenyi Biotec 130–049–101, Auburn,
662 CA), and mixed well. Incubate the cell suspension containing Thy-1 microbeads for 20 min at 4 °C.
663 Mix gently by tapping every 10 min. Add 20 mL of MACS buffer to the tube to dilute Thy-1
664 microbeads and centrifuge at 300 ×g for 10 min at 4 °C. Remove the supernatant completely and
665 resuspend in 2 mL of MACS buffer. Place the separation columns (MS Column; Miltenyi Biotec
666 130-042-201) in the magnetic field of the mini MACS Separation Unit (Miltenyi Biotec 130-142-102)
667 and rinse with 0.5 mL of MACS buffer. Apply the cell suspension to the columns (500μL/ column).
668 After the cell suspension has passed through the column and the column reservoir is empty, wash
669 the column with 0.5mL of MACS buffer three times. Remove the column from the MACS Separation
670 Unit and elute the magnetically retained cells slowly into a 50 mL conical centrifuge tube with 1mL
671 of MACS buffer using the plunger supplied with the column. Centrifuge the tube containing the cells
672 at 600 × g for 10 min at 4 °C and resuspend the cell pellet with 10mL of MACS buffer for rinsing.
673 Repeat this step once. After the final rinsing step, resuspend cells in 0.04% BSA and count the cell
674 number.
675

**Single-cell RNA-seq**

676
677 The MACS-sorted Thy1$^+$ cells were used for loading onto the Chromium Single Cell 3′ Chip kit v2
678 (10x Genomics, PN-120236) according to the instructions. Cell capturing and library preparation
679 was performed following the kit instructions of the Chromium Single Cell 3' v2 Library and Gel Bead
680 Kit (10x Genomics, PN-120237). In brief, 5000 cells were targeted for capture, and after cDNA
681 synthesis, 10-12 cycles were used for library amplification. The libraries were then size-selected,
682 pooled, and sequenced on a Novaseq 6000 (Illumina). Shallow sequencing was performed to
683 access the library quality and to adjust the subsequent sequencing depth based on the capture
684 rate and the detected unique molecular indices (UMI).
685

**Single-cell RNA-seq data processing**

686
687 Raw sequencing reads were processed using the Cell Ranger v.3.0.1 pipeline of the 10x Genomics
688 platform. In brief, reads from each sample were demultiplexed and aligned to the mouse mm10
689 genome, and UMI counts were quantified for each gene per cell to generate a gene-barcode matrix.
690 Default parameters were used. The UMI counts were analyzed using the Seurat R Package (58)
691 (v.3.0.1) following the Seurat pipeline. Cells with more than 200 detected genes or less than 10%
692 mitochondria reads were retained. Genes not detected in at least 10 cells were removed from
693 subsequent analysis. The resulting matrix was normalized, and the most variable genes were found
694 using Seurat's default settings, then the matrix was scaled with regression against the mitochondria
695 reads. The top 2000 variable genes were used to perform PCA, and Jackstraw was performed
696 using Seurat's default settings. Variation in the cells was visualized by UMAP for the top principal
697 components. Cell types were determined using marker genes identified from the literature (59). We
698 used the Seurat function CellCycleScoring to determine the cell cycle phase, as this program
699 determines the relative expression of a large set of G2-M and S-phase genes. After removing the
700 undefined cells, the spermatogonia were used for trajectory analysis, and the single-cell
701 pseudotime trajectory was constructed with the Monocle 2 package (v2.12.0) (60-62) according to
702 the provided documentation. The Monocle function clusterCells was used to detect cell clusters
703 between clusters. The Seurat function FindAllMarkers with default settings was used to find DEGs
704 upregulated in each cluster compared to the other cells. The top200 DEGs of cluster1 were used
705 for ordering cells, and the discriminative dimensionality reduction with trees (DDRTree) method
706 was used to reduce the data to two dimensions. The dynamic expression patterns with the
707 spermatogonial developmental trajectory of specific genes were visualized using the Monocle
708 function plot_genes_in_pseudotime and plot_pseudotime_heatmap. The procession data of the
709 adult human single-cell dataset was downloaded from Gene Expression Omnibus (GEO):
710 GSE112013 and the UMI counts were analyzed using the Seurat R Package (v.3.0.1) following the
711 Seurat pipeline with the same parameters and functions as mentioned previously. According to the
712 known markers, the germ cells characterized was used for trajectory analysis, and the single-cell
713 pseudotime trajectory was constructed with the Monocle 2 package (v2.12.0) as mentioned
714 previously.
715

**CUT & Tag sequencing and analysis**

716
717 CUT&Tag assay was performed using CUT&Tag 2.0 High-Sensitivity Kit (Novoprotein scientific
718 Inc., Cat# N259-YH01). The detailed procedures were described in (40, 63). In brief, cells were
719 harvested by trypsin and enriched by ConA-magnetic beads. 10,000 cells were re-suspended in
720 100 mL Dig-wash Buffer (20 mM HEPES pH 7.5; 150 mM NaCl; 0.5 mM Spermidine; 13 Protease
721 inhibitor cocktail; 0.05% Digitonin) containing 2 mM EDTA and a 1:100 dilution of primary FOXC2
722 antibody. The primary antibody was incubated overnight at 4°C. Beads were washed in Dig-wash

723  Buffer 3 times and incubated with secondary antibody for 1 hour at a dilution of 1:200. After
724  incubation, the beads were washed 3 times in Dig-Hisalt Buffer (0.05% Digitonin, 20 mM HEPES,
725  pH 7.5, 300 mM NaCl, 0.5 mM Spermidine, 13 Protease inhibitor cocktail). Cells were incubated
726  with proteinA-Tn5 transposome at 25°C for 1 h and washed 3 times in Dig-Hisalt buffer to remove
727  unbound proteinA-Tn5. Next, cells were re-suspended in 100mL Tagmentation buffer (10 mM
728  MgCl2 in Dig-Hisalt Buffer) and incubated at 37°C for 1 h. The tagmentation was terminated by
729  adding 2.25 mL of 0.5 M EDTA, 2.75 mL of 10% SDS and 0.5 mL of 20 mg/mL Proteinase K at
730  55°C for 1 hour. The DNA fragments were extracted by phenol chloroform and used for sequencing
731  on an Illumina HiSeq instrument (Illumina NovaSeq 6000) to generate $2 \times 150$-bp paired-end reads
732  following the manufacturer's instructions.
733  Raw reads were analyzed by removing low-quality or adaptor sequences using Trim_galore
734  (v0.5.0) and cleaned reads were mapped to the reference genome mm10 using Bowtie2 (v2.2.5).
735  We used MACS2 (v2.1.2) to call peaks found in different groups. Homer (v4.11.1) de novo motif
736  discovery tool was used for finding the binding motifs of Foxc2 with the findMotifsGenome.pl
737  command. The binding potential of candidate target genes at the binding motif was predicated
738  using the JASPAR Scan function (binding potential >0.8). The peaks filtered by fold change more
739  than 5 and transcription start site (TSS) less than 3000 bp were annotated by R package Chip
740  Seeker for gene category analysis. R package Cluster profiler was used for gene function
741  annotation such as KEGG and GO analysis.
742
743  **Enrichment analyses**
744  Gene Ontology (GO) and KEGG pathway enrichment analyses were conducted using the
745  ClusterProfiler package (v3.12.0) (Yu et al., 2012) and the ClueGO app (v2.5.7) in Cytoscape
746  (v3.8.1) with default settings and a p-value cut-off of 0.05. GSEA enrichment analysis was
747  assessed using the GSEA (v4.0.2) algorithm with MSigDB (v7.0) with default settings. The signaling
748  pathways enriched by niche-derived paracrine factors and undifferentiated SPG-derived
749  membrane proteins in the DEGs of the four samples were characterized. Then for each niche cell
750  type, the niche-derived signaling pathways in all four samples were crossed with the SSC-derived
751  signaling pathways to identify the candidate signaling pathways pivotal to SSCs maintenance.
752
753  **Transplantation assay**
754  The 8-week-old C57BL/6J WT mice were treated with busulfan (40 mg/kg) and used as recipient
755  mice 1 month later. SSCs were transplanted into the testis of recipient mice ($1 \times 10^3$ cells/testis),
756  and two months after transplantation, the testes were harvested and observed under a
757  fluorescence microscope.
758
759  **Fluorescence-activated cell sorting (FACS)**
760  Single-cell suspensions were generated from testes or *in vitro* cultured SSCs. FACS was performed
761  using an SH800 machine (Sony Biotechnology) to isolate the GFP$^+$ cells. Briefly, the GFP$^+$ gating
762  area was based on the point of the fluorescence intensity axis where cells were considered as
763  being GFP$^+$, set based on the background fluorescence intensity of a non-transgenic control testis
764  cell population.
765
766  **Immunofluorescence**
767  Mouse testes were fixed in 4% Paraformaldehyde (PFA) at 4°C overnight, dehydrated, embedded
768  in paraffin, and cut into 5-μm thick sections. The rehydrated mouse or human testis sections were
769  subjected to antigen retrieval, blocked in 5% BSA with 0.1% Triton X-100, and incubated with

770 primary antibody (Supplemental Table S4) at 4°C overnight, including the germ cell marker DDX4,
771 undifferentiated spermatogonia markers ZBTB16, LIN28A, ECAD (64), GFRA1, EOMES, PAX7,
772 progenitor marker NEUROG3, and spermatocyte marker SYCP3 (65). After three 5-min washes in
773 PBS, the sections were incubated with secondary antibodies (Supplemental Table S4) and DAPI
774 (Sigma) at 37°C for 1 h. After three 5-min washes in PBS, coverslips were then mounted on glass
775 slides using anti-quencher fluorescence decay (Solarbio). Images were captured using a Zeiss 780
776 laser-scanning confocal microscope. Whole-mount immunofluorescence of seminiferous tubules
777 was performed as previously described (66). Briefly, seminiferous tubules were disentangled from
778 testicular biopsies and immediately fixed in 4% PFA at 4°C for 12 h. After fixation, the seminiferous
779 tubules were permeabilized with 0.5% Triton X-100 in PBS and treated with 5% BSA in PBS
780 overnight at 4°C. After three 30-min washes, the seminiferous tubules were incubated with primary
781 antibody (Supplemental Table S4) overnight at 4°C. After three 30-min washes, the seminiferous
782 tubules were incubated with species-specific secondary antibodies and DAPI at 4°C for 12 h. After
783 three 30-min washes, the seminiferous tubules were mounted on slides with anti-quencher
784 fluorescence decay (Solarbio) and observed with a Zeiss 780 laser-scanning confocal microscope.
785

786 **RNA isolation and quantitative RT-PCR analysis**
787 Total RNA was extracted from the testes or cultured cells using the RNeasy kit (Qiagen), reverse-
788 transcribed using RevertAid First Strand cDNA Synthesis kit (Thermo), and processed for qRT-
789 PCR using PowerUp SYBR Green Master Mix (Applied Biosystems) and a LightCycler 480 system
790 (Roche) with gene-specific primers (Supplemental Table S4). Reactions were run in triplicate and
791 the mRNA levels were normalized to Gapdh and quantified using the delta-delta Ct method. The
792 values shown are mean ± s.e.m. from three biological replicates.
793

794 **Tamoxifen inducible**
795 According to a previous report for activation of iCre (9), the mice were fed with TD.130859 (TAM
796 diet) for three days. The food was formulated for 400 mg tamoxifen citrate per kg diet, which would
797 provide ~40 mg tamoxifen per kg body weight per day.
798 *Analyses of cyst length.* The cyst length was obtained according to the previous report (67). Briefly,
799 to determine the cyst length, after immunofluorescence staining with anti-E-CAD antibody, the
800 whole mount seminiferous tubule specimens were observed under a fluorescence microscope. The
801 E-CAD staining coupled with staining for FOXC2 enabled us to reliably identify syncytial cysts of
802 FOXC2+ cells.
803

804 **Analyses of cell density**
805 The cell density was counted according to a previous report (68). Briefly, the densities of the
806 ZBTB16+, GFRA1+, LIN28A+, or FOXC2+ cells were measured on the seminiferous tubules with
807 whole-mount staining, the numbers of which per 1000 Sertoli cells were determined.
808

809 **Sperm counts**
810 Total sperm counts were obtained according to the previous report (69). Briefly, epididymal caput
811 and cauda were minced and incubated in prewarmed M16 medium (Sigma-Aldrich) at 37°C in air
812 containing 5% $CO_2$ for 30 min to allow the sperm to swim out. Then, the sperm were diluted in
813 water and counted using a hemocytometer.

**Histology, evaluation of degenerating tubules**

Testes of WT and mutant mice were fixed with PFA fixative and processed for paraffin-embedded section preparation (5 μm thick) and hematoxylin and eosin staining, according to standard procedures. The percentage of degenerating seminiferous tubules was calculated based on the cross-sections of seminiferous tubules (n > 200) that appeared on one transverse section for each testis. In normal (WT) mouse testes, four generations of germ cells, each synchronously progressing through spermatogenesis, form cellular associations of fixed composition (called seminiferous epithelial stages). In the testes of $Foxc2^{flox/-}$; Ddx4-cre mice, a few tubule cross-sections lacked one or more out of the four germ cell layers, which was defined as "degenerative tubules" in this study.

**Statistical analysis**

All statistical analyses were performed using GraphPad Prism (v7.0). All experiments were repeated at least three times, and data for evaluated parameters are reported as mean ± s.e.m. The p-values were obtained using two-tailed unpaired Student's t-tests or one-way ANOVA followed by Tukey test (ns represents p-value > 0.05, * represents p-value < 0.05, ** represents p-value < 0.01, *** represents p-value < 0.001, and **** represents p-value < 0.0001).

**References for Supplemental Materials and Methods**

58. T. Stuart *et al.*, Comprehensive Integration of Single-Cell Data. *Cell* **177**, 1888-1902.e1821 (2019).

59. M. S. Kowalczyk *et al.*, Single-cell RNA-seq reveals changes in cell cycle and differentiation programs upon aging of hematopoietic stem cells. *Genome Res* **25**, 1860-1872 (2015).

60. X. Qiu *et al.*, Reversed graph embedding resolves complex single-cell trajectories. *Nat Methods* **14**, 979-982 (2017).

61. X. Qiu *et al.*, Single-cell mRNA quantification and differential analysis with Census. *Nat Methods* **14**, 309-315 (2017).

62. C. Trapnell *et al.*, The dynamics and regulators of cell fate decisions are revealed by pseudotemporal ordering of single cells. *Nat Biotechnol* **32**, 381-386 (2014).

63. X. Wang *et al.*, N(6)-methyladenosine modification of MALAT1 promotes metastasis via reshaping nuclear speckles. *Dev Cell* **56**, 702-715 e708 (2021).

64. M. Tokuda, Y. Kadokawa, H. Kurahashi, T. Marunouchi, CDH1 is a specific marker for undifferentiated spermatogonia in mouse testes. *Biol Reprod* **76**, 130-141 (2007).

65. L. Yuan *et al.*, The murine SCP3 gene is required for synaptonemal complex assembly, chromosome synapsis, and male fertility. *Mol Cell* **5**, 73-83 (2000).

66. S. Di Persio *et al.*, Spermatogonial kinetics in humans. *Development* **144**, 3430-3439 (2017).

67. T. Nakagawa, M. Sharma, Y. Nabeshima, R. E. Braun, S. Yoshida, Functional hierarchy and reversibility within the murine spermatogenic stem cell compartment. *Science* **328**, 62-67 (2010).

68. R. A. Tegelenbosch, D. G. de Rooij, A quantitative study of spermatogonial multiplication and stem cell renewal in the C3H/101 F1 hybrid mouse. *Mutat Res* **290**, 193-200 (1993).

69. A. Roy, Y. N. Lin, J. E. Agno, F. J. DeMayo, M. M. Matzuk, Absence of tektin 4 causes asthenozoospermia and subfertility in male mice. *Faseb j* **21**, 1013-1025 (2007).

**A** Adult Testis → THY1-beads → MACS → 10X scRNA-seq

**B** Cluster 1 2 3 4 5

**C** Cluster 1 2 3 4 5

*Rasgrp2*
*Tcl1*
*Ppfibp2*
*Chd4*
*Foxc2*
*Mcam*
*Ccnd2*
*Gfra1*
*Rest*
*Egr2*

**D** DAPI/FOXC2/ZBTB16 (Adult)

Whole-mount

Section

**E** FOXC2⁺ cell

- A_s (n=500)
- A_pr (n=500)
- A_pr-1 (n=500)
- A_al4 (n=300)
- A_al8 (n=200)
- A_al16-1 (n=60)

**F** DAPI/FOXC2/MKI67 (Adult)

Proportion/100 FOXC2⁺ cells

MKI67⁺   MKI67⁻

****

**G** Proportion/100 FOXC2⁺ cells

GFRA1⁺  EOMES⁺  PAX7⁺  NEUROG3⁺

FOXC2⁺ proportion/100 cells

GFRA1⁺  EOMES⁺  PAX7⁺  NEUROG3⁺

**H** SSCs / dSPG / SPG / rSPT / eSPT

*FOXC2*   *MKI67*

**I** Celltype    FOXC2⁺    MKI67⁺

**J** Adult human testis

DAPI/FOXC2/ZBTB16        DAPI/FOXC2/MKI67

**A**

*Foxc2^{iCreERT2/+}*;*R26T/G^{f/f}* (2-month-old)

TAM diet

d0  d3  w1  w2  w4  w6  m2  m4  m7  m12

**B** DAPI/GFP/anti-FOXC2 (d3)

**C**

*R26T/G^{f/f}* (TM diet-d3)    GFP+ cells: 0%

*Foxc2^{Cre/+}*;*R26T/G^{f/f}* (TM diet-d3)    GFP+ cells: 0.027%

**D** 2 months after transplantation

THY1+ uSPG    FOXC2+ uSPG

recipient testes

**E**

Colony number / 10³ transplanted cells

THY1+    FOXC2+

****

**F** DAPI/GFP (w1)

a  ZBTB16
b  FOXC2
c  FOXC2  1 2 3
d  FOXC2  1 2
e  FOXC2  1 2 3
f  FOXC2  1 2

**G**

*Foxc2^{Cre/+}*;*R26T/G^{f/f}* (w2)  FOXC2^{GFP}

*Foxc2^{Cre/+}*;*R26T/G^{f/f}* (w4)  FOXC2^{GFP}

*Foxc2^{Cre/+}*;*R26T/G^{f/f}* (w6)  FOXC2^{GFP}

Sperm    Progeny

**I**

Contribution of the GFP+ patches (%)

w6  m2  m4  m7  m12

**J**

Proportion of GFP+ progeny (%)

w6  m2  m4  m7  m12

**H**

*R26T/G^{f/f}* (m4)    *Foxc2^{Cre/+}*;*R26T/G^{f/f}* (m4)

*R26T/G^{f/f}* (m7)    *Foxc2^{Cre/+}*;*R26T/G^{f/f}* (m7)

*R26T/G^{f/f}* (m12)    *Foxc2^{Cre/+}*;*R26T/G^{f/f}* (m12)

Testis  Epididymis    Testis  Epididymis

**K** *Foxc2^{Cre/+}*;*R26T/G^{f/f}* (w2)

DAPI  GFP  EOMES

DAPI  GFP  GFRA1

DAPI  GFP  PAX7

**A** *Foxc2*$^{iCreERT2/+}$;*R26*$^{DTA/+}$ (2-month-old)

TAM diet

d0  d3  d7  d14

**B**

*R26*$^{DTA/+}$    *Foxc2*$^{Cre/+}$;*R26*$^{DTA/+}$    *R26*$^{DTA/+}$    *Foxc2*$^{Cre/+}$;*R26*$^{DTA/+}$

d3                                                    d14

**C**

● *R26*$^{DTA/+}$    ● *Foxc2*$^{Cre/+}$;*R26*$^{DTA/+}$

Testis weight / (g)

ns  ns  *  **

days after TAM diet

Body weight / (g)

ns  ns  ns  ns

days after TAM diet

**D**

cells/1000 sertoli cells

days after tamaxifen treatment

● FOXC2$^+$
● ZBTB16$^+$
● GFRA1$^+$
● LIN28A$^+$

**E**

*R26*$^{DTA/+}$    *Foxc2*$^{Cre/+}$;*R26*$^{DTA/+}$

d3

d14

**F**

DAPI/SYCP3/LIN28A

*R26*$^{DTA/+}$    *Foxc2*$^{Cre/+}$;*R26*$^{DTA/+}$

d14

**G**

Relative mRNA expression

Group
■ *R26*$^{DTA/+}$
■ *Foxc2*$^{Cre/+}$;*R26*$^{DTA/+}$

****  ****  ****  ****  ****  ****  ***  ****

*Foxc2*  *Zbtb16*  *Lin28a*  *Neurog3*  *Gfra1*  *Ret*  *Ddx4*  *Dazl*

**A** 20 days after busulfan treatment (adult) — DAPI/FOXC2/ZBTB16

**B**

Cells number per 1000 sertoli cells vs days after busulfan treatment
- ZBTB16+
- FOXC2+
- GFRA1+

**C** 20 days after busulfan treatment (adult) — DAPI/FOXC2/MKI67

**D**

MKI67+ cells / FOXC2+ cells (%) vs days after busulfan treatment

**E**

$Foxc2^{iCreERT2/+}$;$R26T/G^{f/f}$ (2-month-old)
TAM diet
d0 d3 d20 m2 m4 m7 m12
busulfan

**F** $Foxc2^{iCreERT2/+}$;$R26T/G^{f/f}$ (DAPI/GFP/ZBTB16)
d20    m2

**G**
$R26T/G^{f/f}$ (m4)    $FOXC2^{iCreERT2/+}$;$R26T/G^{f/f}$ (m4)
$R26T/G^{f/f}$ (m7)    $FOXC2^{iCreERT2/+}$;$R26T/G^{f/f}$ (m7)
$R26T/G^{f/f}$ (m12)    $FOXC2^{iCreERT2/+}$;$R26T/G^{f/f}$ (m12)
Testis  Eppididymis    Testis  Eppididymis

**H**

Contribution of the GFP patches (%) vs after busulfan treatment (m2, m4, m7, m12)

**I**

Proportion of GFP+ progeny (%) vs after busulfan treatment (m2, m4, m7, m12)

**A** Wild type allele, Targeting vector, Targeted allele, Knockout allele (Exon1, loxp, Ddx4-Cre)

**B** Foxc2^{f/+}, Foxc2^{f/-};Ddx4-cre — 2M, 6M

**C** Body weight / (g); Testis weight / (g) — ● Foxc2^{f/+} ● Foxc2^{f/-};Ddx4-cre; 2M 3M 4M 5M 6M; ns, ****, ***

**D** Testis, Epididymis — 2M, 6M; Foxc2^{f/+}, Foxc2^{f/-};Ddx4-cre

**E** Degenerative seminiferous tubules (%); Sperm number in epididymis / (×10^7) — ● Foxc2^{f/+} ● Foxc2^{f/-};Ddx4-cre

**F** DAPI/ZBTB16/FOXC2/DDX4 — Foxc2^{f/+}, Foxc2^{f/-};Ddx4-cre; 2M, 6M

**G** Number of ZBTB16^+ cells (per 1000 sertoli cells) — ● Foxc2^{f/+} ● Foxc2^{f/-};Ddx4-cre; 2M 3M 4M 5M 6M

**H** Relative mRNA Expression — ■ Foxc2^{f/+} ■ Foxc2^{f/-};Ddx4-cre; 2M, 6M; Foxc2, Zbtb16, Gfra1, Ret, Ddx4, Dazl

**A** Foxc2^f/+ → THY1-beads → MACS → 10X scRNA-seq → Analysis
Foxc2^f/-;Ddx4-cre

**B** Foxc2^f/+ (CON)    Foxc2^f/-;Ddx4-cre (KO)

Clusters    Clusters

**C** Overall (CON & KO)

CON
KO

other
Cluster1(CON)
Cluster1(KO))

**D** Cells in Cluster1

Cluster1(CON)
Cluster1(KO)

State

**E**

State
1
2
3
4
5

count

CON KO

**F**

CON KO

DEGs in Cluster1 cells

1
0.5
0

**G** The Enriched GO Terms

regulation of binding

stem cell population maintenance

maintenance of cell number

regulation of cellular amide metabolism

in utero embryonic development

regulation of mitotic cell cycle

regulation of translation

epithelial tube morphogenesis

mRNA processing

cytoplasmic translation

−log10(p.adjust)

**H**

Positive regulation of cell cycle process

NOM p-val: 0.4841
FDR q-val: 0.9015
ES: 0.2227
NES: 0.9930

Enrichment Score

cKO v.s. Control

Regulation of cell cycle phase transition

NOM p-val: 0.2831
FDR q-val: 0.8678
ES: 0.2235
NES: 1.0511

Enrichment Score

cKO v.s. Control

**A** Foxc2[iCreERT2/+];R26TG[f/f] (2M)

d0 → TAM diet → d3 → FACS → CUT&Tag_FOXC2

**B** Cut & Tag peaks enriched by FOXC2-antibody from FACS-sorted Foxc2[GFP] cells

Peak enriched region
- Promoter (<=1kb) (48.28%)
- Promoter (1–2kb) (2.74%)
- Promoter (2–3kb) (1.9%)
- 5' UTR (0.33%)
- 3' UTR (1.04%)
- 1st Exon (2.3%)
- Other Exon (2.14%)
- 1st Intron (6.26%)
- Other Intron (11.36%)
- Downstream (<=300) (0.7%)
- Distal Intergenic (22.96%)

**C** CUT&TAG
(TSS)

**D** The Enriched GO Terms
- DNA repair
- ncRNA metabolic process
- regulation of translation
- regulation of mitotic cell cycle
- spindle organization
- methylation
- mitotic nuclear division
- Golgi vesicle transport
- regulation of chromosome organization
- regulation of nuclear division

−log10(p.adjust)

**E** CUT&Tag 3323 — 306 — scRNA-seq 626

**F** Enriched GO Terms
- regulation of mitotic cell cycle
- negative regulation of mitotic cell cycle
- mitotic cell cycle checkpoint

−log10(pvalue)

**G** (genome tracks)
Mad2l1 1kb [0-187]
Bcl2l1 10kb [0-255]
Msh2 10kb [0-220]
Top2b 10kb [0-179]
Angel2 5kb [0-136]
Cdk2ap2 1kb [0-281]
Cenpe 10kb [0-82]
Slc9a3r1 5kb [0-309]
Xpc 5kb [0-190]
Taok3 50kb [0-171]
Btg1 1kb [0-281]

**H** (sequence logo) Probability vs Position

**I** (network diagram)
Cenpe, Xpc, Mad2l1, Cdk2ap2, Top2b, Angel2, Foxc2, Taok3, Msh2, Slc9a3r1, Bcl2l1, Btg1

**J** IgG / FOXC2-antibody
Relative binding Level
Mad2l1, Bcl2l1, Msh2, Top2b, Angel2, Cdk2ap2, Cenpe, Slc9a3r1, Xpc, Taok3, Btg1
****

**K** (schematic)
Regeneration, Homeostasis, Injury, FOXC2+ SSCs pool, Foxc2 Deletion, TA SSCs pool (limited self-renewal), Progenitors, dSPG, Meiosis
FOXC2+ / FOXC2+MKI67+ / FOXC2- uSPG / Fragmentation / Cell death

**A** MACS selected THY1+ cells (DAPI/THY1/ZBTB16)

**B** MACS selected THY1+ cells — THY1− / THY1+

**C** Gfra1, Ret, Eomes, Lhx1, Lhx2, Egr2, Upp1, Nanos3, Neurog3, Sox3, Kit, Stra8

**D** Cluster 1 2 3 4 5 — Ret, Lhx1, Lhx2, Gfra1, Egr2, Upp1, Sox3, Neurog3, Nanos3, Sohlh1, Stra8, Kit, Sohlh2

**E** Pseudotime — Ret, Lhx1, Lhx2, Gfra1, Egr2, Upp1, Sox3, Neurog3, Nanos3, Sohlh1, Stra8, Kit, Sohlh2

**F** Cluster 1 2 3 4 5 — Cell cycle genes (S, G2M)

**G** Pseudotime

**A**

Rasgrp2, Tcl1, Ppfibp2, Chd4, Foxc2, Mcam, Ccnd2, Gfra1, Rest, Egr2 (violin plots with Expression Level on y-axis and Cluster 1–5 on x-axis)

Rasgrp2, Tcl1, Ppfibp2, Chd4, Foxc2, Mcam, Ccnd2, Rest (t-SNE feature plots)

**B**

DAPI/LIN28A

RASGRP2, PPFIBP2, CHD4, CCND2, REST (immunofluorescence images)

**C**

UTF1, ID4, FGFR3, PIWIL4, TSPAN33, TCF3, EGR4 (t-SNE feature plots)

L1TD1, GFRA1, EGR4, STRA8, SOX4, DMRT1, MAGEA4 (t-SNE feature plots)

**A**

*Foxc2* Wild type allele

5'UTR    3'UTR
Exon1

Targeting vector

iCreERT2
-WPRE-pA

*Foxc2* Targeted allele

iCreERT2
-WPRE-pA

**B**

DAPI/ZBTB16/FOXC2/DDX4

$R26^{DTA/+}$

$Foxc2^{Cre/+};R26^{DTA/+}$

d3

$R26^{DTA/+}$

$Foxc2^{Cre/+};R26^{DTA/+}$

d14

**A**



DAPI/ZBTB16/LIN28A/TRA98 (1 Week)

*Foxc2^{f/+}*

*Foxc2^{f/-}; Ddx4-cre*

**B**

DAPI/LIN28A/Cleaved-CASP3 (2M)

*Foxc2^{f/+}*

*Foxc2^{f/-};Ddx4-cre*

**A**

Foxc2^f/+ (CON)

Foxc2  Ret  Gfra1

Upp1  Sox3  Stra8

Egr2  Zbtb16  Kit

Lhx1  Sohlh2  Sall4

Foxc2^f/−;Ddx4-cre (KO)

Eomes  Ret  Gfra1

Upp1  Sox3  Stra8

Egr2  Zbtb16  Kit

Lhx1  Sohlh2  Sall4

**B**

Pseudotime of CON

Foxc2
Ret
Gfra1
Lhx1
Egr2
Upp1
Sox3
Stra8
Sohlh2
Kit

−3 −2 −1 0 1 2 3

Pseudotime of KO

Eomes
Ret
Gfra1
Lhx1
Egr2
Upp1
Sox3
Stra8
Sohlh2
Kit

−3 −2 −1 0 1 2 3

**C**

Pseudotime of overall

Foxc2
Ret
Gfra1
Lhx1
Egr2
Upp1
Sox3
Stra8
Sohlh2
Kit

−3 −2 −1 0 1 2 3

**A**

Sample
- ● *Foxc2^{f/+}*  ● *Foxc2^{f/-}; Ddx4*-cre

Subcluster
- ● 0  ● 1

**B**

Count vs Subcluster (0, 1)

Sample
- *Foxc2^{f/+}*
- *Foxc2^{f/-};Ddx4*-cre

**C**

*Foxc2*  *Ret*  *Gfra1*  *Lhx1*

*Upp1*  *Sox3*  *Stra8*  *Sohlh2*

*Egr2*  *Zbtb16*  *Kit*  *Sall4*

**D**

Cells in Cluster1

0 → 1  Subcluster

Pseudotime

**E**

Pseudotime →

*Ret*
*Gfra1*
*Lhx1*
*Egr2*
*Upp1*
*Sox3*
*Stra8*
*Kit*

−3 −2 −1 0 1 2 3